IDE**▲**L®

Directional Wavelets Revisited: Cauchy Wavelets and Symmetry Detection in Patterns

J.-P. Antoine

Institut de Physique Théorique, Université Catholique de Louvain, B-1348 Louvain-la-Neuve, Belgium

E-mail: antoine@fyma.ucl.ac.be

R. Murenzi

CTSPS and Department of Physics, Clark Atlanta University, Atlanta, Georgia 30314

E-mail: murenzi@hubble.cau.edu

and

P. Vandergheynst[1]

Institut de Physique Théorique, Université Catholique de Louvain, B-1348 Louvain-la-Neuve, Belgium

E-mail: Pierre.Vandergheynst@epfl.ch

The analysis of oriented features in images requires two-dimensional directional wavelets. Among these, we study in detail the class of Cauchy wavelets, which are strictly supported in a (narrow) convex cone in spatial frequency space. They have excellent angular selectivity, as shown by a standard calibration test, and they have minimal uncertainty. In addition, we present a new application of directional wavelets, namely a technique for determining the symmetries of a given pattern with respect to rotations and dilation. © 1999 Academic Press

1. INTRODUCTION

As is well known [12], the wavelet transform (WT) comes in two very different incarnations, based on mutually exclusive philosophies, namely the continuous WT

---

[1] Current address: Signal Processing Lab. LTS/DE, EPFL, CH-1015 Lausanne, Switzerland.

(CWT) and the discrete or dyadic WT (DWT). According to conventional wisdom, the CWT is better adapted for the analysis of signals, in particular feature detection, whereas the DWT is preferred for signal synthesis and data compression. The reason is that the DWT leads to orthonormal or biorthogonal wavelet bases, and (bi)orthogonality ensures a maximal decorrelation among the wavelet coefficients.

Specializing to the two-dimensional case, the 2-D CWT will be used mainly for detection, extraction, or classification of various features in images. But then a further choice must be made. If the aim is a pointwise analysis, without particular emphasis on directions, then an isotropic wavelet, such as the isotropic Mexican hat, will be more economical. But if the features to be detected have a preferred direction (straight edges, filaments, oriented textures, velocity field, etc.), then one needs a wavelet with good angular selectivity. In [2], we have defined a *directional wavelet* as a wavelet $\psi(\vec{x})$ whose Fourier transform $\hat{\psi}(\vec{k})$ has (essential) support in a convex cone in spatial frequency space, with apex at the origin. The canonical example, of course, is the 2-D Morlet wavelet. Up to Gaussian tails, it lives in an ellipse centered on the wave vector $\vec{k}_0$, and hence contained in the convex cone defined by the tangents to that ellipse. The detection capability of the Morlet wavelet has been thoroughly analyzed in [1, 2] and it has been characterized by two parameters, the scale resolving power (SRP) and the angular resolving power (ARP). Taken together, these two parameters define a tiling of the spatial frequency plane, thus leading to the determination of a complete filter bank suitable for image analysis.

However, the Morlet wavelet has a drawback. In order to make it more directionally selective, one must increase $|\vec{k}_0|$ (in addition to increasing the anisotropy parameter ϵ, which results in a further elongating of the supporting ellipse). But there is a price to pay. When $|\vec{k}_0|$ increases, the amplitude of $\hat{\psi}(\vec{k})$ diminishes, since it contains a factor $\exp(-|\vec{k}_0|^2)$. Thus one has to find a directional compromise and keep $|\vec{k}_0|$ within reasonable bounds, which implies that the ARP of the Morlet wavelet is in fact limited.

As an alternative to the Morlet wavelet, we have introduced in [2] another class of directional wavelets, namely the *Cauchy wavelets*. They are strictly contained in a convex cone in $\vec{k}$-space, with a fully controllable opening angle, independently of the amplitude. They have an arbitrary large number of vanishing moments on the boundary of the supporting cone and an exponential decay inside (alternatively, one may impose a Gaussian decay). These Cauchy wavelets generalize to two (or more) dimensions the wavelets of Paul [13, 30, 31] (actually, they were introduced by Klauder [27] and the name "Cauchy" was given by Holschneider [22]).

One of the purposes of this paper is to study the 2-D Cauchy wavelets in a systematic way, both mathematically (Section 2) and in terms of their performances for analysis (Section 3). In addition, we will show in Section 4 that the Cauchy wavelets have *minimal uncertainty,* in the sense that they saturate the uncertainty relations that result from the nonvanishing commutation relations among some of the infinitesimal generators of the transformations defining the 2-D CWT, namely translations, dilations, and rotations (see [1]). This property is familiar in the 1-D case, where it was introduced by Gabor [16] in his pioneering work on time–frequency analysis. The fact that the Gaussian has minimal uncertainty, either in the sense of quantum mechanics (Heisenberg uncertainty relations) or in the sense of signal processing (which is the same thing), has been invoked time and again for justifying its preeminent role, both in Gabor analysis and in wavelet analysis.

In the final Section 5, we describe an application of directional wavelets that looks extremely promising. We introduce the so-called *scale-angle measure* of an object, namely the space integral of the square modulus of its WT, which may also be interpreted as the (partial) energy density of the CWT in the scale and angle variables. Using this concept, we show that a directional wavelet, for instance a Cauchy wavelet, is able to determine the symmetry of a given object in a straightforward way. This applies to geometrical figures (a square, a hexagon), but also to tilings, which may have both a rotational symmetry and a combined rotation–dilation symmetry. It is revealing that the tiling that was used for detecting a rotational symmetry (of order 8) had also such a combined symmetry—but the latter was discovered on the scale-angle measure, *not* on the tiling itself. We expect this technique to be useful, for instance, in the study of quasi-crystals and other patterns with approximate symmetries.

We conclude this Introduction by fixing our conventions and recalling the basic definitions concerning the 2-D CWT. An image is a finite energy signal $s \in L^2(\mathbb{R}^2, d^2\vec{x})$. A wavelet is a signal $\psi \in L^2(\mathbb{R}^2, d^2\vec{x})$ satisfying the familiar admissibility condition

$$c_\psi \equiv (2\pi)^2 \int \frac{d^2\vec{k}}{|\vec{k}|^2} |\hat{\psi}(\vec{k})|^2 < \infty \tag{1.1}$$

(we will put $c_\psi = 1$ throughout). If ψ is regular enough ($\psi \in L^1(\mathbb{R}^2, d^2\vec{x}) \cap L^2(\mathbb{R}^2, d^2\vec{x})$ suffices), the admissibility condition simply means that the wavelet has zero mean:

$$\hat{\psi}(\vec{0}) = 0 \Leftrightarrow \int d^2\vec{x} \, \psi(\vec{x}) = 0. \tag{1.2}$$

Given an image $s \in L^2(\mathbb{R}^2, d^2\vec{x})$, its wavelet transform (with respect to the fixed wavelet ψ) $S \equiv W_\psi s$ is given, as usual, by the scalar product of s with the transformed wavelet $\psi_{\vec{b},a,\theta}$, considered as a function of $(\vec{b}, a, \theta)$:

$$S(\vec{b}, a, \theta) = \langle \psi_{\vec{b},a,\theta} | s \rangle \tag{1.3}$$

$$= a^{-1} \int d^2\vec{x} \, \bar{\psi}(a^{-1}r_{-\theta}(\vec{x} - \vec{b}))s(\vec{x}) \tag{1.4}$$

$$= a \int d^2\vec{k} \, e^{i\vec{b}\cdot\vec{k}} \overline{\hat{\psi}}(ar_{-\theta}(\vec{k}))\hat{s}(\vec{k}). \tag{1.5}$$

In these relations, $\vec{b} \in \mathbb{R}^2$ is the displacement parameter, $a > 0$ the dilation parameter, and θ the rotation angle, and the rotation $r_\theta \in SO(2)$ acts on $\vec{x} = (x, y)$ in the usual way.

It is a basic aspect of the CWT that the transformed wavelet $\psi_{\vec{b},a,\theta}$ is obtained from ψ by a unitary operator $U(\vec{b}, a, \theta)$, which defines a square integrable representation of the two-dimensional Euclidean group with dilations, i.e., the similitude group SIM(2) of $\mathbb{R}^2$,

$$\psi_{\vec{b},a,\theta}(\vec{x}) \equiv a^{-1}\psi(a^{-1}r_{-\theta}(\vec{x} - \vec{b})) = (U(\vec{b}, a, \theta)\psi)(\vec{x}), \qquad (1.6)$$

or, equivalently, in the space of Fourier transforms,

$$\widehat{\psi_{\vec{b},a,\theta}}(\vec{k}) \equiv ae^{-i\vec{b}\cdot\vec{k}}\hat{\psi}(ar_{-\theta}(\vec{k})) = (\hat{U}(\vec{b}, a, \theta)\hat{\psi})(\vec{k}). \qquad (1.7)$$

The formula (1.7) will be used in Section 4 for determining the effect of infinitesimal transformations, that is, the representation of the Lie algebra sim(2) acting on wavelets.

2. MATHEMATICAL PROPERTIES OF THE CAUCHY WAVELETS

2.1. Directional Wavelets

In frequency space, the 1-D (Cauchy) wavelets of Paul have the following form, with $m > 0$:

$$\hat{\psi}_m(\omega) = \begin{cases} 0, & \text{for } \omega < 0, \\ \omega^m e^{-\omega}, & \text{for } \omega \geq 0. \end{cases} \qquad (2.1)$$

Now, in 1-D, the positive half-line is a convex cone. Thus a natural generalization to 2-D will be a wavelet whose support in spatial frequency space is contained in a convex cone with apex at the origin. This is exactly the definition of a *directional* wavelet that we introduced in [1], with the purpose of characterizing wavelets capable of detecting oriented features (segments, edges, vector field, etc.) in images (a review of directional wavelets and their use may be found in [3]).

Since it may sound counterintuitive, this definition requires a word of justification. According to (1.5), the wavelet acts as a filter in $\vec{k}$-space (multiplication by the function $\hat{\psi}$). Suppose the signal $s(\vec{x})$ is strongly oriented, for instance, a long segment along the positive x-axis. Then its Fourier transform $\hat{s}(\vec{k})$ is a long segment along the positive k_y-axis. In order to detect such a signal, with a good directional selectivity, one needs a wavelet ψ supported in a narrow cone in $\vec{k}$-space. Then the WT is negligible unless $\hat{\psi}(\vec{k})$ is essentially aligned onto $\hat{s}(\vec{k})$: directional selectivity demands restriction of the support of $\hat{\psi}$, not ψ. In the same way, in signal processing, restrictions on the support of filters are imposed in the *frequency* domain (high pass, band pass, etc.). A case in point is the analysis of *textures* with directional wavelets. Both in [18] and in [24, 29] the algorithm demands that the wavelet $\hat{\psi}$ be well localized in spatial frequency space. In particular, its (essential) support must be contained in a rather narrow cone. Notice that a discrete version of wavelet analysis with a Morlet wavelet (called Gabor wavelet!) has been used previously in texture analysis [25], with very good reconstruction results. On the contrary, spatial localization properties of the directional wavelets are not important. Indeed, the wavelets of Paul have a poor localization in the time domain (they decrease as an inverse power for $t \to \pm\infty$).

The best known directional wavelet is, of course, the 2-D Morlet wavelet that we have analyzed in detail in [1]. Strictly speaking, it is only approximately directional, since it has

Gaussian tails outside the cone of its essential support, but this makes no difference numerically. Another example of directional wavelet has been proposed by Watson [39]. His fan filters are obtained by taking first the difference between two "mesa" functions, which yields an angular wavelet, and then repeatedly bisecting the spatial frequency space and taking only one side (i.e., the associated analytic signal). The allowed directions θ are thus restricted to a fan-shaped region:

$$0 \leq 2\theta \leq \frac{2\pi}{2^{n-1}} \ (n = 2, 3, \dots). \tag{2.2}$$

This construction may then be generalized to arbitrary angles [32]. These fan filters have all the properties of directional wavelets, including admissibility in the form (1.2). Applying to these filters discrete rotations and scaling, Watson builds a pyramid of oriented filters as a tool for data compression and signal reconstruction after coding, in a model of human vision. This is, in fact, a discretized version (in polar geometry) of the CWT. Another example, very similar to the previous one, is that of the *steerable filters,* introduced by Freeman and Adelson [15], and further developed by Perona [33] and Simoncelli *et al.* [34]. Here again one obtains a multiscale pyramid decomposition, which is quite efficient in a number of problems, mostly related to machine vision. Similar techniques have been used with the Gabor transform [25].

By comparison with these (and related) works, the present paper shows two main differences. First, we use the precise mathematical definition of *directional wavelet* introduced in [2]. Accordingly, while (analytic) fan filters are directional, in the strict sense, steerable filters cannot be, although they may be approximately directional, just like the Morlet wavelet. For instance, the simplest example given in [15] is a filter based on directional derivatives. Thus it is not supported in a convex cone and therefore is not directional, although it is an oriented wavelet. Second, we are interested in feature detection and analysis. For this purpose, it is more efficient to use the continuous WT than the discrete one, as illustrated, for instance, in [18] and in [24, 29]. In particular, instead of using a dyadic discretization scheme (scaling by powers of 2), we use first a continuous scaling, and the values chosen for the eventual discretization are arbitrary and, in fact, dictated by the signal itself (as in the analysis of fractals [5, 6]). In that sense, we are closer to the scale-space philosophy of Witkin [42].

2.2. Cauchy Wavelets

With these preliminary remarks in mind, we may now proceed to the definition of the new wavelets. Let $\mathscr{C} \equiv \mathscr{C}(\alpha, \beta)$ be the convex cone determined by the unit vectors $\vec{e}_\alpha, \vec{e}_\beta$, where $\alpha < \beta$, $\beta - \alpha < \pi$ and $\vec{e}_\gamma \equiv (\cos \gamma, \sin \gamma)$. The axis of the cone is $\vec{\zeta}_{\alpha\beta} = \vec{e}_{(1/2)(\alpha+\beta)}$. Then one has

$$\mathscr{C}(\alpha, \beta) = \{\vec{k} \in \mathbb{R}^2 : \alpha \leq \arg(\vec{k}) \leq \beta\}$$

$$= \{\vec{k} \in \mathbb{R}^2 : \vec{k} \cdot \vec{\zeta}_{\alpha\beta} \geq \vec{e}_\alpha \cdot \vec{\zeta}_{\alpha\beta} = \vec{e}_\beta \cdot \vec{\zeta}_{\alpha\beta} > 0\}. \tag{2.3}$$

The dual cone, also convex, is

$$\tilde{\mathscr{C}} \equiv \mathscr{C}(\tilde{\alpha}, \tilde{\beta}) = \{\vec{k} \in \mathbb{R}^2, \vec{k} \cdot \vec{k}' > 0, \ \forall \, \vec{k}' \in \mathscr{C}(\alpha, \beta)\}, \tag{2.4}$$

where $\tilde{\beta} = \alpha + \pi/2$, $\tilde{\alpha} = \beta - \pi/2$, and therefore $\vec{e}_{\tilde{\alpha}} \cdot \vec{e}_{\beta} = \vec{e}_{\tilde{\beta}} \cdot \vec{e}_{\alpha} = 0$, whereas $\vec{e}_{\tilde{\alpha}} \cdot \vec{e}_{\alpha} = \vec{e}_{\tilde{\beta}} \cdot \vec{e}_{\beta} = \sin(\beta - \alpha)$. Thus the axis of $\tilde{\mathscr{C}}$ is $\vec{\zeta}_{\alpha\beta}$ again. (It might seem more natural to use the variables $\check{\alpha} = \tilde{\beta}$, $\check{\beta} = \tilde{\alpha}$, as was done in [2], but the present definition makes things more symmetric and has the further advantage of extending to higher dimensions, as we shall see in a while.)

In these notations, we define a 2-D *Cauchy wavelet,* with support in $\mathscr{C} = \mathscr{C}(\alpha, \beta)$, for any $\vec{\eta} \in \tilde{\mathscr{C}}$ and $l, m \in \mathbb{N}^*$, through its Fourier transform:

$$\hat{\psi}_{lm}^{(\mathscr{C}, \vec{\eta})}(\vec{k}) = \begin{cases} (\vec{k} \cdot \vec{e}_{\tilde{\alpha}})^l (\vec{k} \cdot \vec{e}_{\tilde{\beta}})^m e^{-\vec{k} \cdot \vec{\eta}}, & \vec{k} \in \mathscr{C}(\alpha, \beta), \\ 0, & \text{otherwise.} \end{cases} \tag{2.5}$$

Clearly this function satisfies the admissibility condition (1.1) for 2-D wavelets. In addition, the Cauchy wavelet itself, in position space, may also be obtained explicitly (this result was announced, without proof, in [2]). Indeed:

PROPOSITION 2.1. *For every $\vec{\eta} \in \tilde{\mathscr{C}}$ and $l, m \in \mathbb{N}^*$, the 2-D Cauchy wavelet $\psi_{lm}^{(\mathscr{C}, \vec{\eta})}(\vec{x})$ with support in $\mathscr{C} = \mathscr{C}(\alpha, \beta)$ belongs to $L^2(\mathbb{R}^2, d\vec{x})$ and is given by*

$$\psi_{lm}^{(\mathscr{C}, \vec{\eta})}(\vec{x}) = \frac{i^{l+m+2}}{2\pi} \, l! m! \, \frac{[\sin(\beta - \alpha)]^{l+m+1}}{[(\vec{x} + i\vec{\eta}) \cdot \vec{e}_{\alpha}]^{l+1} [(\vec{x} + i\vec{\eta}) \cdot \vec{e}_{\beta}]^{m+1}}. \tag{2.6}$$

Proof. From the definition (2.5), we get

$$\psi_{lm}^{(\mathscr{C}, \vec{\eta})}(\vec{x}) = \frac{1}{2\pi} \int_{\mathscr{C}(\alpha,\beta)} d^2\vec{k} \, e^{i\vec{k} \cdot \vec{x}} (\vec{e}_{\tilde{\alpha}} \cdot \vec{k})^l (\vec{e}_{\tilde{\beta}} \cdot \vec{k})^m e^{-\vec{k} \cdot \vec{\eta}}$$

$$= \frac{(-i)^{l+m}}{2\pi} [\vec{e}_{\tilde{\alpha}} \cdot \vec{\nabla}_{\vec{x}}]^l [\vec{e}_{\tilde{\beta}} \cdot \vec{\nabla}_{\vec{x}}]^m \int_{C(\alpha,\beta)} d^2\vec{k} \, e^{-\vec{k} \cdot (\vec{\eta} - i\vec{x})}.$$

The integral on the rhs is convergent, since $\vec{k} \cdot \vec{\eta} > 0$. Write $\vec{\xi} = \vec{\eta} - i\vec{x} = -i(\vec{x} + i\vec{\eta})$ and let A be the matrix that maps the unit vectors $\vec{e}_1$, $\vec{e}_2$ onto $\vec{e}_{\alpha}$, $\vec{e}_{\beta}$, respectively: $(\vec{e}_{\alpha})^i = A^i_{\alpha}(\vec{e}_j)^i$, so that $k^j = A^j_{\nu} k^{\nu}$ (contravariant coordinates, $\nu = \alpha, \beta$). Explicitly, we have

$$A = \begin{pmatrix} \cos \alpha & \cos \beta \\ \sin \alpha & \sin \beta \end{pmatrix}, \qquad \text{so that } \det A = \sin(\beta - \alpha).$$

In the new (nonorthogonal) coordinates, the cone becomes

$$\mathscr{C}(\alpha, \beta) = \{\vec{k} \in \mathbb{R}^2 : k^{\alpha} \geq 0, \, k^{\beta} \geq 0\},$$

and the integral may be obtained immediately:

$$\int_{\mathscr{C}(\alpha,\beta)} d^2\vec{k}\, e^{-\vec{k}\cdot\vec{\xi}} = \int_{\mathscr{C}(\alpha,\beta)} dk^1 dk^2 \exp(-A^j_\nu k^\nu \xi_j)$$

$$= \det A \int_0^\infty dk^\alpha \int_0^\infty dk^\beta \exp(-k^\nu \xi_\nu), \qquad \text{where } \xi_\nu = A^j_\nu \xi_j$$

$$= \frac{\det A}{\xi_\alpha \xi_\beta} = \frac{\sin(\beta - \alpha)}{(\vec{e}_\alpha \cdot \vec{\xi})(\vec{e}_\beta \cdot \vec{\xi})} = \frac{-\sin(\beta - \alpha)}{[(\vec{x} + i\vec{\eta}) \cdot \vec{e}_\alpha][(\vec{x} + i\vec{\eta}) \cdot \vec{e}_\beta]}.$$

Then the result follows by differentiation, if one remembers that $\vec{e}_{\tilde\alpha} \cdot \vec{e}_\beta = \vec{e}_{\tilde\beta} \cdot \vec{e}_\alpha = 0$. Indeed,

$$(\vec{e}_{\tilde\beta} \cdot \vec{\nabla}_{\tilde{x}}) \frac{1}{[(\vec{x} + i\vec{\eta}) \cdot \vec{e}_\alpha]} = \frac{\vec{e}_{\tilde\beta} \cdot \vec{e}_\alpha}{[(\vec{x} + i\vec{\eta}) \cdot \vec{e}_\alpha]^2} = 0,$$

$$(\vec{e}_{\tilde\beta} \cdot \vec{\nabla}_{\tilde{x}})^m \frac{1}{[(\vec{x} + i\vec{\eta}) \cdot \vec{e}_\beta]} = \frac{(-1)^m m! (\vec{e}_{\tilde\beta} \cdot \vec{e}_\beta)^m}{[(\vec{x} + i\vec{\eta}) \cdot \vec{e}_\beta]^{m+1}} = \frac{(-1)^m m! [\sin(\beta - \alpha)]^m}{[(\vec{x} + i\vec{\eta}) \cdot \vec{e}_\beta]^{m+1}},$$

and similarly for the other factor. As for the square integrability of the resulting function, it is obvious. ∎

In the symmetric case $l = m$, (2.6) may be rewritten

$$\psi_{mm}^{(\mathscr{C},\vec{\eta})}(\vec{x}) = \frac{(-1)^{m+1}}{2\pi} (m!)^2 \frac{[\sin(\beta - \alpha)]^{2m+1}}{[(\vec{x} + i\vec{\eta}) \cdot \sigma(\alpha, \beta)(\vec{x} + i\vec{\eta})]^{m+1}}, \qquad (2.7)$$

where

$$\sigma(\alpha, \beta) = \begin{pmatrix} \cos\alpha \cos\beta & \sin(\alpha + \beta) \\ \sin(\alpha + \beta) & \sin\alpha \sin\beta \end{pmatrix}.$$

Two remarks are in order here. First we notice that Eq. (2.6) may be rewritten in the form

$$\psi_{lm}^{(\mathscr{C},\vec{\eta})}(\vec{x}) = \text{const.}(\vec{z} \cdot \vec{e}_\alpha)^{-l-1}(\vec{z} \cdot \vec{e}_\beta)^{-m-1}, \qquad (2.8)$$

where we have introduced the complex variable $\vec{z} = \vec{x} + i\vec{\eta} \in \mathbb{R}^2 + i\tilde{\mathscr{C}}$. Thus the Cauchy wavelet is *separable,* albeit in a geometry where the coordinate axes are taken along $\vec{e}_\alpha$, $\vec{e}_\beta$.

Then, if we vary $\vec{\eta} \in \tilde{\mathscr{C}}$, the expression (2.8) shows that $\psi_{lm}^{(\mathscr{C},\vec{\eta})}$ extends to an analytic function of z. This follows from general theorems [36, 37]. Since the function $\hat{\psi}_{lm}^{(\mathscr{C},\vec{\eta})}(\vec{k})$ has support in the convex cone $\mathscr{C} = \mathscr{C}(\alpha, \beta)$ and is of fast decrease at infinity, its Fourier transform $\psi_{lm}^{(\mathscr{C},\vec{\eta})}(\vec{x})$ is the boundary value of a function $\psi_{lm}^{(\mathscr{C})}(\vec{z})$, holomorphic in the tube $\mathbb{R}^2 + i\tilde{\mathscr{C}}$. What we have here is in fact an example of a 2-D progressive wavelet.

In 1-D, a wavelet ψ is called *progressive* or a Hardy function [19, 22], if $\hat{\psi}(\omega) = 0$ for $\omega < 0$. This in turn may be expressed in terms of the Hilbert transform, defined by $\widehat{Hf}(\omega) = -i \operatorname{sign} \omega f(\omega)$, namely

$$\psi = (1 + iH)\phi, \quad \phi \in L^2(\mathbb{R}, dt)$$

(that is, ψ is the analytic signal associated to ϕ). Equivalently, ψ belongs to the Hardy space $H_+^2(\mathbb{R})$ of square integrable functions which extend analytically into the upper half-plane. We claim that the directional wavelets are the 2-D analogues of this concept, that is, the genuine 2-D progressive wavelets.

In order to prove that statement, we first notice that the convex cone $\mathcal{C}(\alpha, \beta)$ may also be expressed in terms of the covariant coordinates $k_{\bar{\nu}} = (\vec{e}_{\bar{\nu}} \cdot \vec{k})$, $\nu = \alpha, \beta$:

$$\mathcal{C}(\alpha, \beta) = \{\vec{k} \in \mathbb{R}^2 : k_{\bar{\alpha}} \geq 0, \ k_{\bar{\beta}} \geq 0\}. \tag{2.9}$$

Consider the directional Hilbert transforms:

$$\widehat{H_{\bar{\nu}}f}(\vec{k}) = -i \operatorname{sign} k_{\bar{\nu}} f(\vec{k}). \tag{2.10}$$

Given $\phi \in L^2(\mathbb{R}^2, d^2\vec{x})$, define the function

$$\psi = (1 + iH_{\bar{\alpha}} + iH_{\bar{\beta}} - H_{\bar{\alpha}}H_{\bar{\beta}})\phi = (1 + iH_{\bar{\alpha}})(1 + iH_{\bar{\beta}})\phi. \tag{2.11}$$

Then it is easy to see, as in [38], that $\hat{g}(\vec{k})$ vanishes outside the cone $\mathcal{C}(\alpha, \beta)$, and indeed,

$$\hat{\psi}(\vec{k}) = \begin{cases} 4\hat{\phi}(\vec{k}), & \vec{k} \in \mathcal{C}(\alpha, \beta), \\ 0, & \text{otherwise.} \end{cases} \tag{2.12}$$

Therefore the inverse Fourier transform $\psi(\vec{x})$ is the boundary value of a function $\psi(\vec{z})$ holomorphic in the tube $\mathbb{R}^2 + i\widetilde{\mathcal{C}}$, that is, a 2-D Hardy function. For a fixed convex cone $\mathcal{C}(\alpha, \beta)$, the set of all such functions constitutes a Hilbert space, naturally denoted $H_{(\alpha,\beta)}^2$, which is unitary equivalent, via the complex Fourier transform, to the space $L^2(\widetilde{\mathcal{C}}(\alpha, \beta), d^2\vec{k})$ [36, Thm. VI.3.1]. In this sense, directional wavelets are a genuine multidimensional generalization of the 1-D Hardy functions, much more so than the so-called 2-D Hardy functions defined by Dallard and Spedding [11]. And among them Cauchy wavelets are particularly simple (they occupy a special niche, as we will see in Section 4). Two concluding remarks are in order: first, all these considerations extend to higher dimensions $n > 2$; second, we are talking here of a Hardy space $H_{(\alpha,\beta)}^2$, but similar considerations may be made for Hardy spaces $H_{(\alpha,\beta)}^1$, in terms of the Riesz operators that are a natural multidimensional generalization of the Hilbert transform [38].

Let us give a few examples of 2-D Cauchy wavelets. For simplicity, we always take $\vec{\eta}$ along $\vec{\zeta}_{\alpha\beta}$, the axis of the cone. In this case, for $l = m$, the wavelet, written $\psi_{mm}^{(\mathcal{C})}(\vec{x})$, is symmetric under reflection with respect to $\vec{\eta}$.

Take first $\mathscr{C}_1 = \mathscr{C}(0, \pi/2)$ and $\vec{\eta} = \vec{e}_{\pi/4} = (1, 1)$. Then, for $l = m = 1$, one gets the function

$$\psi_{11}^{(\mathscr{C}_1)}(\vec{x}) = \frac{1}{2\pi} \frac{1}{(x + i)^2} \frac{1}{(y + i)^2}, \tag{2.13}$$

i.e., the product of two 1-D Cauchy wavelets [22, 30], that is, derivatives of the Cauchy kernel $(z + i)^{-1}$—hence the name.

Similarly, for any $m \geq 1$, we get

$$\psi_{mm}^{(\mathscr{C}_1)}(\vec{x}) = \frac{(-1)^{m+1}}{2\pi} (m!)^2 \frac{1}{(x + i)^{m+1}} \frac{1}{(y + i)^{m+1}}. \tag{2.14}$$

These wavelets are indeed symmetric under reflection in the main diagonal, $x \leftrightarrow y$, and they are separable in the usual sense.

On the other hand, for $\mathscr{C}_2 = \mathscr{C}(\pi/4, 3\pi/4)$, we obtain

$$\psi_{mm}^{(\mathscr{C}_2)}(\vec{x}) = \frac{(-1)^{m+1}}{2\pi} (m!)^2 \frac{1}{(u + i\eta_u)^{m+1}} \frac{1}{(v + i\eta_v)^{m+1}}, \tag{2.15}$$

where we have introduced the (light-cone) coordinates $u = 2^{-1/2}(x + y)$, $v = 2^{-1/2}(-x + y)$. In the axisymmetric case, $\vec{\eta} = (0, 1)$, this gives

$$\psi_{mm}^{(\mathscr{C}_2)}(\vec{x}) = \frac{(-1)^{m+1}}{2\pi} (m!)^2 \left[\frac{1}{(y + i)^2 - x^2} \right]^{m+1}, \tag{2.16}$$

which is indeed an even function of x.

Of course, in practical applications, one needs a reasonable directional selectivity, and therefore one chooses a narrower supporting cone. Indeed, for a Cauchy wavelet, the ARP, the parameter that measures the directional selectivity, as defined in [1], is simply the opening angle of the cone, $\Phi = \beta - \alpha$. We have found that $\mathscr{C}_{10} = \mathscr{C}(-10°, 10°)$ is a good choice (this will be confirmed by the calibration analysis given in Section 3 below). In addition, imposing sufficiently many vanishing moments also improves the performances of the wavelet, as usual. We show in Fig. 1 the wavelet $\hat{\psi}_{44}^{(\mathscr{C}_{10})}(\vec{k})$; this is manifestly a highly directional filter.

An alternative possibility is to replace in (2.5) the exponential by a Gaussian centered on the axis of the cone, $\exp(-|\vec{k} - a_0\vec{\zeta}_{\alpha\beta}|^2)$ $(a_0 > 0)$. The resulting wavelet is very similar to the previous one, except that it is more concentrated in spatial frequency space, since it is also sharply localized in scale, around the central scale a_0. We show an example in Fig. 2. In the applications of Section 5, we use both $\psi_{44}^{(\mathscr{C}_{10})}$ and its Gaussian analogue, and the difference in scale selectivity between the two will be manifest.

As a final remark, let us note that the definition (2.5) extends immediately to three or more dimensions. In 3-D, we consider the convex simplicial (or pyramidal) cone
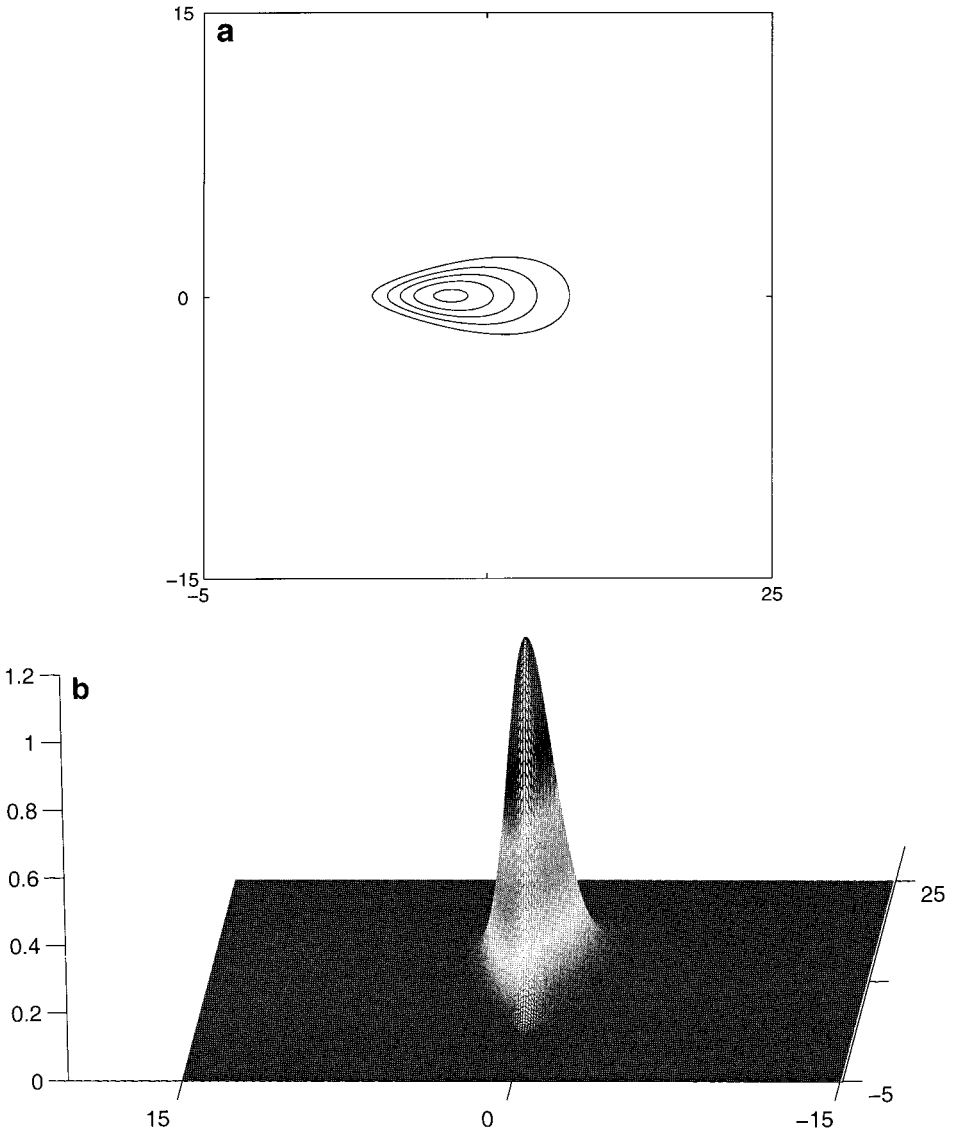
FIG. 1. The Cauchy wavelet $\hat{\psi}_{44}^{(\mathscr{C}_{10})}(\vec{k})$ in spatial frequency space: (a) in level curves; (b) a 3-D view from $\theta = 185°$.

$\mathscr{C}(\alpha, \beta, \gamma)$ defined by the three unit vectors $\vec{e}_\alpha$, $\vec{e}_\beta$, $\vec{e}_\gamma$, the angle between any two of them being smaller than π. The dual cone is also simplicial, namely $\tilde{\mathscr{C}} = \mathscr{C}(\tilde{\alpha}, \tilde{\beta}, \tilde{\gamma})$, where $\vec{e}_{\tilde{\alpha}} = \vec{e}_\beta \wedge \vec{e}_\gamma$ is orthogonal to the β–γ face, etc. With these notations, given a vector $\vec{\eta} \in \tilde{\mathscr{C}}$ and $l, m, n \in \mathbb{N}^*$, we define a 3-D Cauchy wavelet in spatial frequency space as

$$\hat{\psi}_{lmn}^{(\mathscr{C}, \vec{\eta})}(\vec{k}) = \begin{cases} (\vec{k} \cdot \vec{e}_{\tilde{\alpha}})^l (\vec{k} \cdot \vec{e}_{\tilde{\beta}})^m (\vec{k} \cdot \vec{e}_{\tilde{\gamma}})^n e^{-\vec{k} \cdot \vec{\eta}}, & \vec{k} \in \mathscr{C}(\alpha, \beta, \gamma), \\ 0, & \text{otherwise.} \end{cases} \quad (2.17)$$
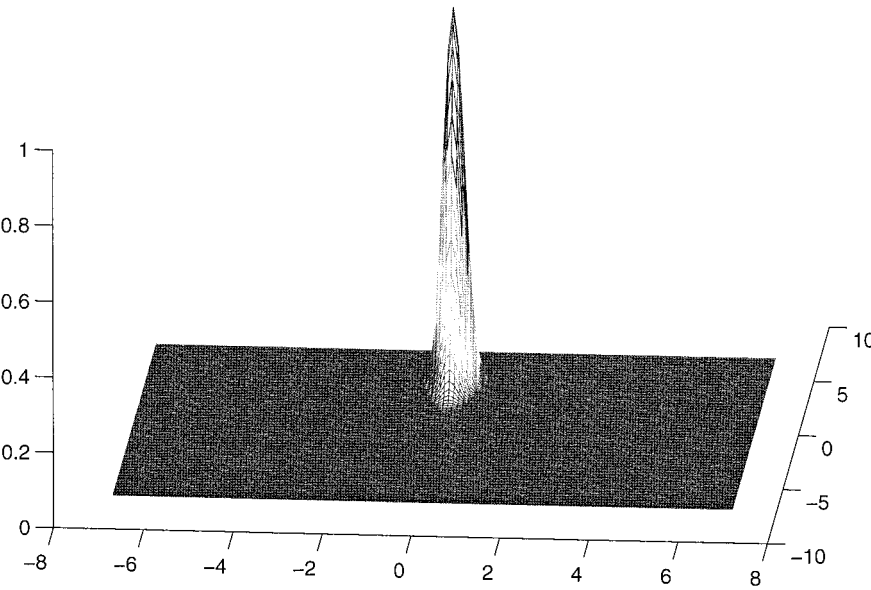
FIG. 2. A Gaussian Cauchy wavelet, with support in the cone $\mathscr{C}_{10}$, $l = m = 4$, $a_0 = 1$.

Then, with exactly the same proof as for Proposition 2.1, we get the explicit expression for the 3-D wavelet in position space,

$$\psi_{lmn}^{(\mathscr{C},\vec{\eta})}(\vec{x}) = \frac{i^{l+m+n+3}}{2\pi}\, l!m!n! \cdot \det A \cdot \frac{(\vec{e}_{\tilde{\alpha}} \cdot \vec{e}_{\alpha})^{l}(\vec{e}_{\tilde{\beta}} \cdot \vec{e}_{\beta})^{m}(\vec{e}_{\tilde{\gamma}} \cdot \vec{e}_{\gamma})^{n}}{(\vec{z} \cdot \vec{e}_{\alpha})^{l+1}(\vec{z} \cdot \vec{e}_{\beta})^{m+1}(\vec{z} \cdot \vec{e}_{\gamma})^{n+1}}, \tag{2.18}$$

where, as in the 2-D case, A is the matrix that transforms the unit vectors into the triple $\vec{e}_{\alpha}$, $\vec{e}_{\beta}$, $\vec{e}_{\gamma}$ and we have written $\vec{z} = \vec{x} + i\vec{\eta}$. All the other comments remain valid. From the expressions (2.17) and (2.18), one may then obtain other 3-D Cauchy wavelets, for instance, one supported in a circular cone. And the whole construction extends to any number of dimensions.

3. CALIBRATION OF THE CAUCHY WAVELET

It is clear from Fig. 1 that, if the supporting cone is narrow enough, the Cauchy wavelet is a highly directional filter. But, of course, for practical applications, we must convert this assertion into quantitative terms. In other words, the wavelet must be *calibrated.*

As for any directional wavelet, the crucial property is directional selectivity. In order to estimate this, we submit the Cauchy wavelet to the same test that we used in [1] for the Morlet wavelet. The test (benchmark) signal is a semi-infinite rod, sitting along the positive x-axis, and modeled as usual with a delta function,
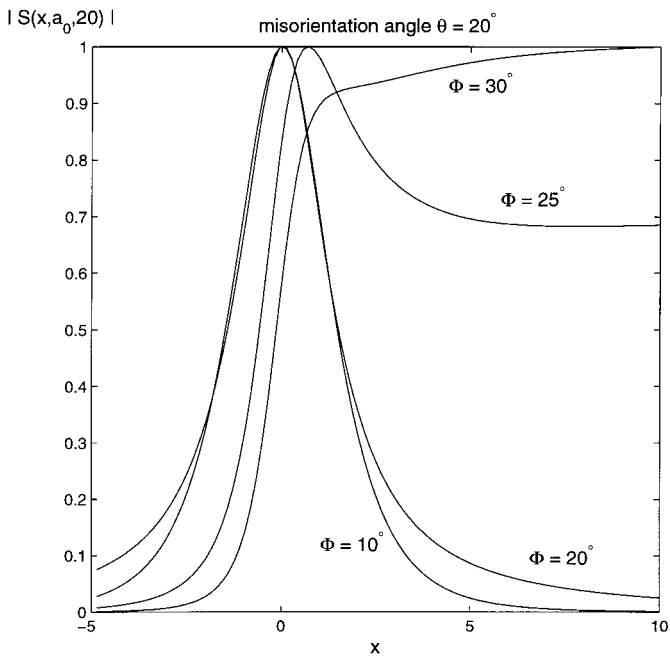
$$s(\vec{x}) = \vartheta(x)\delta(y), \tag{3.1}$$
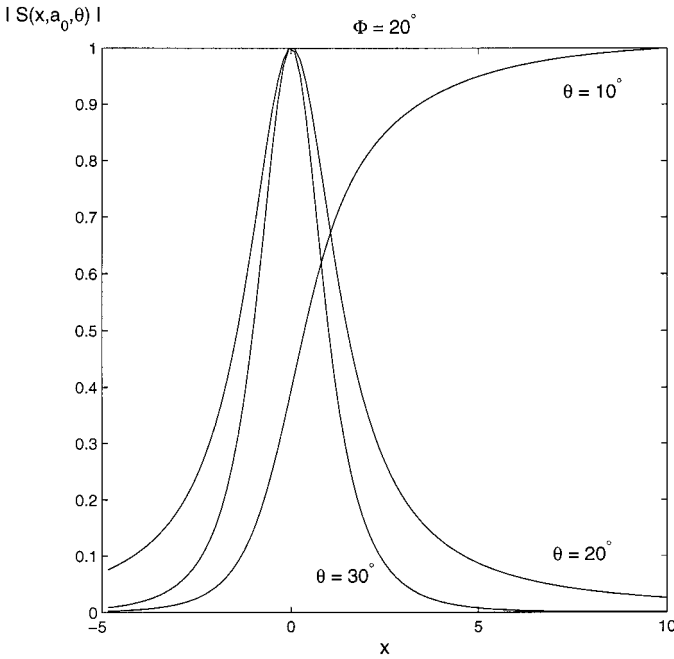
FIG. 3. Angular selectivity of $\hat{\psi}_{44}^{(\mathscr{C}_{10})}$ as a function of the misorientation angle θ. The graph shows the modulus $|S(x, a_0, \theta)|$ as a function of position x along the rod, for various values of θ.

where $\vartheta(x)$ is the step function. Then one takes a Cauchy wavelet and computes the modulus of the CWT of s as a function of x, for the fixed scale $a_0 = 1$ and orientation θ. Thus θ is the "misorientation" of the wavelet with respect to the signal (the rod). As expected, the result is entirely similar to that obtained in [1] for the Morlet wavelet. This is shown in Fig. 3 for a Cauchy wavelet supported in the cone $\mathscr{C}_{10} = \mathscr{C}(-10°, 10°)$, with axis $\vec{\eta} = (1, 0)$, that is, an angular resolving power $\Phi = 20°$. For $\theta = 0$, the modulus of the WT is a "wall," increasing smoothly from 0, for $x \leq -5$, to its asymptotic value (normalized to 1) for $x \geq 5$. Then, for increasing misorientation θ, the wall gradually collapses and essentially disappears for $\theta > 10°$. Only the tip of the rod remains visible, and for large θ ($\theta > 45°$), it gives a sharp peak. This is exactly the property used crucially in the measurement of the velocity field of a turbulent fluid [3, 40, 41].

Thus, on this count, the Cauchy wavelet behaves exactly as the Morlet wavelet. But it has in fact an additional advantage. In the Morlet case, tightening the supporting cone means increasing the modulus of the wave vector $\vec{k}_0$, but this also means decreasing the amplitude, because $\vec{k}_0$ enters in the exponent of the Gaussian. Thus $\vec{k}_0$ cannot be taken too large. For the Cauchy wavelet, on the contrary, the opening angle of the cone Φ and the amplitude of the wavelet are almost independent parameters. The latter decreases very slowly as $\Phi \to 0$, as a fixed power of $\sin \Phi$. Thus one may take a cone as narrow as one wishes, with almost constant amplitude. As an example, we show in Fig. 4 the result of narrowing the cone, for a fixed misorientation angle $\theta = 20°$ between the wavelet and the rod. Of course, exactly the same conclusion applies to the Gaussian version of the Cauchy wavelet.

The outcome of this analysis is that Cauchy wavelets, with a narrow supporting cone, are excellent directional wavelets. They are easier to implement than the 2-D Morlet

FIG. 4. Angular selectivity of $\hat{\psi}_{44}^{(\mathscr{C}_{10})}$ as a function of the opening angle Φ of the cone $\mathscr{C}$. The graph shows the modulus $|S(x, a_0, 20°)|$ as a function of x, for various values of Φ.

wavelet and have a fully controllable angular selectivity. As shown above, a Cauchy wavelet with opening angle $\Phi = 20°$ is a good replacement for the usual 2-D Morlet wavelet with $|\vec{k}_0| = 5.5$, and in our group we are now using that kind of wavelet almost exclusively.

4. CAUCHY WAVELETS HAVE MINIMAL UNCERTAINTY

4.1. Minimal Wavelets

In his pioneering paper on time–frequency analysis, Gabor [16] stresses the notion of a signal with minimal uncertainty. The latter is defined as the product of the variances of the position and the frequency, in other words, the product of the widths of the signal in the time and the frequency variables. It is always bounded below, as a result of the Fourier theorem, and the minimal uncertainty signals are those for which the lower bound is attained. This concept is identical to that of uncertainty in a quantum mechanical system, which is governed by the celebrated Heisenberg relations [9, 17]. For the usual time–frequency pair, the minimum is reached for a Gaussian signal, a fact that is often invoked for justifying its choice, in particular by Gabor himself (the "elementary signal") [16].

Now, in the standard case, the time and frequency widths are simply the variances of the operators of infinitesimal modulation and translation, respectively. In other words, finding the signal with minimal uncertainty is a Lie algebra problem, in a Hilbert space representation. For the canonical case, the Lie algebra in question is, of course, that of the canonical commutation relations. Let us formulate the problem in precise mathematical terms.

Let A and B be two densely defined, essentially self-adjoint operators of a Hilbert space with scalar product $\langle \cdot | \cdot \rangle$. Let ϕ be a normalized vector ($\|\phi\| = 1$) in the domains of both A and B. The variance of A in the state ϕ is defined as

$$\Delta A \equiv \Delta_\phi A = \sqrt{\langle A^2 \rangle - \langle A \rangle^2}, \tag{4.1}$$

where $\langle C \rangle = \langle \phi | C\phi \rangle$ denotes the average of the operator C in the state ϕ. Then we have the well-known proposition.

PROPOSITION 4.1. *Let A, B, and ϕ be as above. Then one has*

$$\Delta A \cdot \Delta B \geq \frac{1}{2} |\langle [A, B] \rangle|. \tag{4.2}$$

The equality holds in (4.2) *iff*

$$(A - \langle A \rangle)\phi = -i\lambda_0 (B - \langle B \rangle)\phi, \tag{4.3}$$

for some $\lambda_0 > 0$.

The proof can be found in Gabor's paper [16] or in any standard quantum mechanics textbook, for instance [9, 17]. Note that $A = -i\dfrac{d}{dx}$ and $B = x$ gives the usual Heisenberg inequalities, that is, the canonical case discussed above. A state ϕ which saturates the inequality (4.2), that is, which verifies (4.3), is called a state of *minimal uncertainty,* or sometimes an intelligent state [28]. In the Heisenberg case, one gets of course the familiar canonical coherent states.

In the case of more than two operators, one obtains a system of inequalities, one for each nonvanishing commutator.

4.2. Two-Dimensional Minimal Wavelets

Coming back to 1-D wavelets, we have to remember that a^{-1} plays the role of a frequency. Thus the operators to consider for applying Proposition 4.1 are the infinitesimal generators of dilations and translations, in the unitary representation of the $ax + b$ group that underlies wavelet theory. This was first done by Klauder [27], and then by Paul and Seip [30, 31] and by Dahlke and Maass [10], with the result that the 1-D Cauchy–Paul wavelets (and their generalizations defined in the Appendix of [13]) have minimal uncertainty. In the 2-D wavelet case, Dahlke and Maass have considered the isotropic solutions only and found that the 2-D isotropic Mexican hat is a minimal uncertainty wavelet.

Let us consider the case of a general 2-D wavelet. It is well known [1–3] that the four-dimensional parameter space of the 2-D CWT is in fact the phase space associated to the similitude group of the plane. The variable $\vec{b}$ in (1.3) represents the position, whereas the pair (a^{-1}, θ) is interpreted as spatial frequency in polar coordinates. This is the basis for the privileged role played by the two standard representations of the CWT, the position and the scale-angle representation, described at length in [1–3]. Thus, by the

same principle as in the 1-D case, the analogue of the canonical uncertainty relations is obtained by considering the commutators between infinitesimal generators of translations, on the one hand, and dilations and rotations, on the other.

In order to formulate this in a mathematically precise way, we consider the representation $\hat{U}$ in the Fourier variables, as given in (1.7), and denote the infinitesimal generators by P_1 for horizontal translations, P_2 for vertical translations, D for dilations, and J for rotations. Then we have, with $\vec{k} = (k_x, k_y) \equiv (\rho, \varphi)$:

$$(P_1\hat{\psi})(\vec{k}) = i\,\frac{d}{db_x}\,(\hat{U}(\vec{b}, a, \theta)\hat{\psi})(\vec{k})|_{(1,0,\vec{0})} = k_x\hat{\psi}(\vec{k}), \tag{4.4}$$

$$(P_2\hat{\psi})(\vec{k}) = i\,\frac{d}{db_y}\,(\hat{U}(\vec{b}, a, \theta)\hat{\psi})(\vec{k})|_{(1,0,\vec{0})} = k_y\hat{\psi}(\vec{k}), \tag{4.5}$$

$$(D\hat{\psi})(\vec{k}) = i\,\frac{d}{da}\,(\hat{U}(\vec{b}, a, \theta)\hat{\psi})(\vec{k})|_{(1,0,\vec{0})}$$

$$= i(k_x\partial_{k_x} + k_y\partial_{k_y} + 1)\hat{\psi}(\vec{k}) = i(\rho\partial_\rho + 1)\hat{\psi}(\rho, \varphi), \tag{4.6}$$

$$(J\hat{\psi})(\vec{k}) = i\,\frac{d}{d\theta}\,(\hat{U}(\vec{b}, a, \theta)\hat{\psi})(\vec{k})|_{(1,0,\vec{0})}$$

$$= -i(k_x\partial_{k_y} - k_y\partial_{k_x})\hat{\psi}(\vec{k}) = -i\partial_\varphi\hat{\psi}(\rho, \varphi). \tag{4.7}$$

The corresponding commutation relations are

$$[P_1, P_2] = 0; \quad [D, P_1] = iP_1; \quad [J, P_1] = iP_2;$$
$$[D, J] = 0; \quad [D, P_2] = iP_2; \quad [J, P_2] = -iP_1. \tag{4.8}$$

PROPOSITION 4.2. *The four nonzero commutators split in two sets of two commutators,*

$$[D, P_1] = iP_1; \qquad [J, P_2] = -iP_1, \tag{4.9}$$

and

$$[D, P_2] = iP_2; \qquad [J, P_1] = iP_2, \tag{4.10}$$

that transform into each other under the transformation $\varphi \mapsto \varphi - \pi/2$.

Proof. In fact the considered transformation leaves D and J invariant, whereas (P_1, P_2) go into $(P_2, -P_1)$. ∎

Thus it suffices to consider minimal wavelets for one pair of commutation relations; we shall choose (4.9) and write the corresponding system of inequalities. We obtain

$$\Delta D \cdot \Delta P_1 \geq \tfrac{1}{2}|\langle P_1\rangle|$$

$$\Delta J \cdot \Delta P_2 \geq \tfrac{1}{2}|\langle P_1\rangle|. \tag{4.11}$$

According to the second statement in Proposition 4.1, a vector $\hat{\psi}$ saturates the lower bound of the above inequalities if and only if

$$(D + i\lambda_1 P_1)\hat{\psi}(\vec{k}) = (\langle D\rangle + i\lambda_1\langle P_1\rangle)\hat{\psi}(\vec{k})$$
$$(J + i\lambda_2 P_2)\hat{\psi}(\vec{k}) = (\langle J\rangle + i\lambda_2\langle P_1\rangle)\hat{\psi}(\vec{k}) \qquad (\lambda_1, \lambda_2 > 0). \tag{4.12}$$

In polar coordinates, this system reads

$$(\rho\partial_\rho + 1 + \lambda_1\rho \cos \varphi)\hat{\psi}(\rho, \varphi) = -i\beta_1\hat{\psi}(\rho, \varphi)$$

$$(-\partial_\varphi + \lambda_2\rho \sin \varphi)\hat{\psi}(\rho, \varphi) = -i\beta_2\hat{\psi}(\rho, \varphi), \tag{4.13}$$

where

$$\beta_1 = \langle D\rangle + i\lambda_1\langle P_1\rangle, \qquad \beta_2 = \langle J\rangle + i\lambda_2\langle P_2\rangle. \tag{4.14}$$

The integrability of the system (4.13) requires that $\lambda_1 = \lambda_2 \equiv \lambda > 0$. Then the general solution is given by

$$\hat{\psi}(\rho, \varphi) = c\rho^{-i\beta_1-1}e^{i\beta_2\varphi}e^{-\lambda\rho \cos \varphi}. \tag{4.15}$$

The solution (4.15) must verify the following three conditions:

(1) 2π-*periodicity in* φ implies that

$$\beta_2 = \langle J\rangle + i\lambda\langle P_2\rangle = m, \qquad m \in \mathbb{Z},$$

which in turn requires

$$\langle P_2\rangle = \int\int d^2\vec{k}k_y|\hat{\psi}(\vec{k})|^2 = 0 \qquad \text{and} \qquad \langle J\rangle = m \in \mathbb{Z}.$$

Thus, introducing $\kappa_1 \equiv \lambda\langle P_1\rangle - 1$ and $\kappa_2 \equiv -\langle D\rangle$, the solution (4.15) becomes

$$\hat{\psi}(\rho, \varphi) = c\rho^{\kappa_1+i\kappa_2}e^{-im\varphi}e^{-\lambda\rho \cos \varphi}. \tag{4.16}$$

(2) *Square integrability* implies that k_x must be restricted to positive values only, which means

$$\cos \varphi > 0 \Leftrightarrow |\varphi| \leq \varphi_0 < \pi/2. \tag{4.17}$$

Therefore the wavelet ψ is square integrable iff the support of its Fourier transform is restricted to a convex cone in the right half-plane. In addition, one needs $\kappa_1 > -1$.

(3) *Admissibility:* Inserting the solution (4.16) in the admissibility integral (1.1), with the condition (4.17), we obtain

$$c_\psi < (2\pi)^3 \int_0^\infty \rho^{2\kappa_1-1} e^{-2\lambda\rho\cos\varphi_0} d\rho. \tag{4.18}$$

The convergence of this integral then requires $\kappa_1 > 0$.

Assume now $\hat\psi(\vec k)$ to be real. Then $\langle J \rangle = \langle D \rangle = 0$. Indeed,

$$\langle J \rangle = \frac{1}{i} \int_0^\infty \rho d\rho \int_0^{2\pi} d\varphi \hat\psi(\rho, \varphi) \partial_\varphi \hat\psi(\rho, \varphi) = \frac{1}{2i} \int_0^\infty \rho d\rho \int_0^{2\pi} d\varphi \partial_\varphi |\hat\psi(\rho, \varphi)|^2 = 0,$$

since $\hat\psi$ is 2π-periodic. Hence we must have $m = 0$.

In the same way,

$$\langle D \rangle = \int_0^{2\pi} d\varphi \int_0^\infty d\rho (\rho^2 \hat\psi(\rho, \varphi) \partial_\rho \hat\psi(\rho, \varphi) + \rho |\hat\psi(\rho, \varphi)|^2)$$

$$= \frac{1}{2} \int_0^{2\pi} d\varphi (\rho^2 |\hat\psi(\rho, \varphi)|^2)|_0^\infty = 0,$$

since $\hat\psi$ is in the domain of D.

Thus we may state

PROPOSITION 4.3. *A real wavelet $\hat\psi$ is minimal with respect to the commutation relations* (4.9) *iff it vanishes outside some convex cone $\mathscr{C}$ in the half-plane $k_x > 0$ and is exponentially decreasing inside:*

$$\hat\psi(\vec k) = \begin{cases} c|\vec k|^\kappa e^{-\lambda \vec k \cdot \vec e_1} \ (\kappa > 0, \lambda > 0), & \vec k \in \mathscr{C}, \\ 0, & otherwise. \end{cases} \tag{4.19}$$

If we had chosen the pair (4.10) instead, we would have obtained a convex cone in the lower half-plane $\vec k \cdot \vec e_2 < 0$. Combining the two results, we see that the wavelet $\hat\psi$ is minimal with respect to the commutation relations (4.9) and (4.10) iff its support is contained in the lower right quarter-plane, $\vec k \cdot \vec e_1 > 0$, $\vec k \cdot \vec e_2 < 0$. Since the whole construction is rotation invariant, this in turn means that the opening angle of the supporting cone must be strictly smaller than $\pi/2$. Thus we state:

PROPOSITION 4.4. *A real wavelet $\hat\psi$ has minimal uncertainty iff it vanishes outside some convex cone $\mathscr{C}$ with apex at the origin and opening angle $\Phi < \pi/2$, and is exponentially decreasing inside:*

$$\hat\psi(\vec k) = \begin{cases} c|\vec k|^\kappa e^{-\lambda \vec k \cdot \vec\eta} \ (\kappa > 0, \lambda > 0, \vec\eta \in \tilde{\mathscr{C}}), & \vec k \in \mathscr{C} \\ 0, & otherwise. \end{cases} \tag{4.20}$$

In other words, $\hat{\psi}$ must be of the form

$$\hat{\psi}(\vec{k}) = c\chi_c(\vec{k})|\vec{k}|^\kappa e^{-\lambda\vec{k}\cdot\vec{\eta}} \qquad (\kappa > 0,\ \lambda > 0), \qquad (4.21)$$

where χ_c is the characteristic function of $\mathscr{C}$, or a smoothened version thereof.

We may now impose some degree of regularity (vanishing moments) at the boundary of the cone, by taking an appropriate linear superposition of such minimal wavelets $\hat{\psi}$. Thus we obtain finally

$$\hat{\psi}^{\mathscr{C}}(\vec{k}) = c\chi_c(\vec{k})F(\vec{k})e^{-\lambda\vec{k}\cdot\vec{\eta}} \qquad (\lambda > 0), \qquad (4.22)$$

where $F(\vec{k})$ is a polynomial in k_x, k_y, vanishing at the boundaries of the cone $\mathscr{C}$, including the origin. Clearly a Cauchy wavelet with $\Phi < \pi/2$ is of this type.

Note that other minimal wavelets may be obtained if one includes commutators with elements of the enveloping algebra of the Lie algebra (4.8). For instance, taking the commutator between D and the Laplacian $-\Delta = P_1^2 + P_2^2$, one finds a whole family of minimal isotropic wavelets, among them all powers of the Laplacian, Δ^n, acting on a Gaussian [4]. For $n = 2$, this gives the 2-D isotropic Mexican hat [10]. There exist more general solutions of the minimizing equations, but most of them are not square integrable.

As a conclusion of this section, we might say that the minimal uncertainty property is an important attribute of 2-D wavelets, exactly as in 1-D. What is important is not the localization in position alone, but the *simultaneous* localization in position $\vec{b}$ and scale orientation (a, θ), that is, the localization in phase space. This is precisely the property that is optimized by the minimal wavelets given in Proposition 4.4, since they achieve equality in all four uncertainty relations derived from the commutation relations (4.9) and (4.10). Thus minimal wavelets are as optimal for the 2-D wavelet transform as the Gabor function is for the Gabor or windowed Fourier transform, and for the same reason. The Cauchy wavelets are thus linear combinations of optimal wavelets. However, this is a theoretical statement, and it is not clear to us whether it implies an operational meaning. For instance, the 2-D Morlet wavelet and Gaussian Cauchy wavelets are not minimal, yet they are extremely powerful for directional analysis. This is not new: in 1-D, too, the Cauchy–Paul wavelet (2.1) is minimal, but many other ones are at least as useful in practice, for instance, the derivatives of the Gaussian or the Morlet wavelet.

As a last remark, it may be interesting to notice that a concept closely related to minimality has been developed by Simoncelli *et al.* [35] under the name of *jointly shiftable filters*. First, shiftable filters are the natural generalization of steerable filters to variables other than rotations, such as translation or scaling. Then a filter is jointly shiftable in two variables simultaneously iff the corresponding operations commute ("are independent"). Thus strict joint shiftability is impossible for position and spatial frequency, and only approximately shiftable filters exist. And the optimal ones, that is, those that minimize the "joint aliasing," are the same as our minimal wavelets.

In any case, whatever the answer to the question of the operational meaning of minimality, if any, we emphasize that we are using the Cauchy wavelets *not* because they are minimal, but simply because they are simpler to implement and more efficient than, say, the Morlet wavelets (although they have a slower decay in position space).

5. DETERMINING SYMMETRIES IN IMAGES AND 2-D PATTERNS

In general, directional wavelets are used for detecting oriented features in an image, for instance, the vectors of the velocity field in a turbulent fluid [3, 40, 41] or oriented textures [18, 24, 29], and they are quite efficient in that respect. In this section we will describe another application that uses in an essential way the angular selectivity of the directional wavelets, and we shall illustrate it with the Cauchy wavelet. Namely, we shall present a simple method that allows one to evaluate the symmetry of a given object, and even possibly a local or an approximate symmetry. Let $S(\vec{b}, a, \theta)$ be the wavelet transform of the signal $s(\vec{x})$ with respect to a directional wavelet. On the space of transforms, we introduce the following positive valued function:

$$\mu_S(a, \theta) = \int d\vec{b} |S(\vec{b}, a, \theta)|^2 \tag{5.1}$$

$$= (2\pi a)^2 \int d^2\vec{k} |\hat{\psi}(ar_{-\theta}(\vec{k}))|^2 |\hat{s}(\vec{k})|^2. \tag{5.2}$$

We call μ_s the *scale-angle measure* of the signal. This is different from using the scale-angle representation [1, 2], which consists in fixing the position parameter $\vec{b}$. Here, on the contrary, μ_s averages over all points in the plane, in order to eliminate the dependence on the point of observation. This is a further confirmation of the fact that the localization properties in position space are unimportant for such applications. One may also interpret μ_s as the (partial) energy density of the signal in the scale and angle variables, that is, in spatial frequency space, according to the phase space interpretation of the CWT given in [1, 2]. From the properties of the wavelet transform, it is clear that, for any signal s of finite energy and any smooth wavelet, μ_s is a bounded continuous function of a and θ. Furthermore, if ψ is directional, $\hat{\psi}$ is supported in a narrow cone, and then (5.2) "probes" the behavior of the signal in the direction θ, as the beam of a torchlight exploring a target. This intuitively explains all the results that follow.

We begin with a simplified version and eliminate the scale dependence by integrating over a, thus ending with a function $\alpha_s(\theta)$ of the rotation angle only, called the *angular measure* of the object. In general, α_s is 2π-periodic. But when the analyzed object has rotational symmetry n, that is, it is invariant under a rotation of angle $2\pi/n$, then the angular measure is in fact $2\pi/n$-periodic. Note that, for $n = 2$, there are two different operations of order 2, rotation of π and reflection (mirror symmetry), which may also be seen as a rotation of π around an axis lying in the plane of the figure (Ox or Oy).

To give some examples, we consider simple geometrical figures (Fig. 5). Take first a square, which has symmetry $n = 4$. The angular measure $\alpha_s(\theta)$ is thus $2\pi/4$-periodic and shows four equal, equidistant peaks at $\theta = 0°, 90°, 180°, 270°$. The width of these peaks is simply the aperture of the cone $\mathscr{C} = \mathscr{C}(\alpha, \beta)$, namely $\mathscr{C}_{10}$ in the example considered (more generally, the ARP of the wavelet). Similarly, a regular hexagon has symmetry $n = 6$, and thus its angular measure shows six equal peaks. The case of the rectangle is more interesting. It has symmetry $n = 2 \times 2$ (two mirror symmetries, or rotations by π around both Ox or Oy), and this is reflected on the graph of its angular measure. There are two large peaks corresponding to the directions of the longest edges and two smaller ones
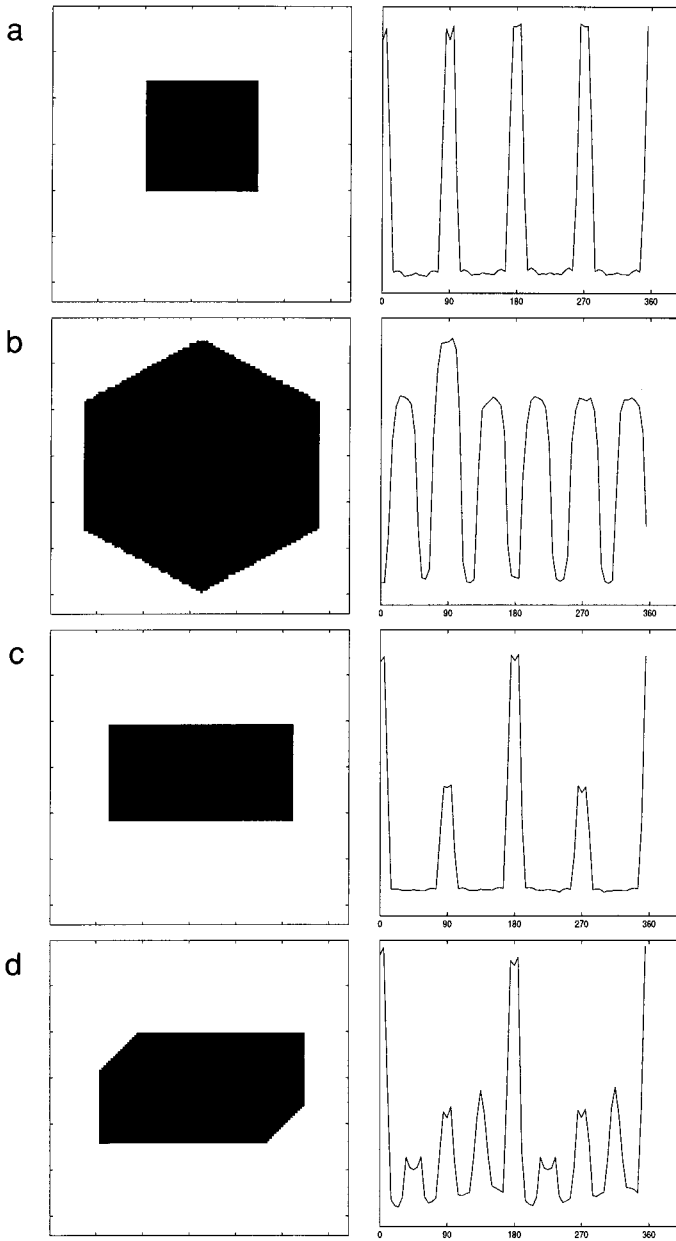
FIG. 5. Angular measure $\alpha_s(\theta)$ of some geometrical figures: (a) a square; (b) a hexagon; (c) a rectangle with symmetry 2×2; (d) a truncated rectangle, with symmetry 2.

corresponding to the directions of the shortest edges, and the ratio 2:1 between the two equals the ratio of the lengths of the corresponding edges. In contrast, for a truncated rectangle, which has only one symmetry (rotation by π around Oz), the angular measure $\alpha_s(\theta)$ shows only two main peaks, at $\theta = 0°$ and $180°$ (smaller ones are visible, corresponding to the other, shorter edges).

Of course, these examples are toy problems that can be solved by plenty of methods, and they are included here only in order to check the validity of the approach in the case of a pure rotational symmetry. However using the full scale-angle measure (5.1), (5.2) leads us much further. This technique also allows one to identify the combined rotation–dilation symmetries of quasilattices or tilings. In order to test this, we show in Fig. 6 the analysis of a known "twisted snowflake." This means a mathematical snowflake [5, 6] with the following modified construction rule: Upon each downscaling by a factor of 3, the figure is turned by $36°$. The scale-angle measure of this object, computed with a Cauchy wavelet $\psi_{44}^{(\mathcal{C}_{10})}$, shows precisely the combined symmetry. The set of four maxima at a given scale a_0 is reproduced, at scale $a_0/3$, but translated in θ by $36°$. And reconstructing the WT at the values (a, θ) corresponding to these maxima yields successive approximations of the original signal, as with the usual snowflake.

Let us turn now to a nontrivial example, whose symmetries are not obvious, namely the octagonal tiling given in Fig. 7a. It has a global symmetry $n = 8$, as shown in Fig. 7b, and is invariant, by construction, under dilation by a factor $1 + \sqrt{2}$. But one may go further and uncover combined rotation–dilation symmetries of the tiling, with the help of its scale-angle measure $\mu_s(a, \theta)$. This time we use a Gaussian Cauchy wavelet ($l = m = 4$), in order to get a better scale localization. The result is plotted in Fig. 8a (only half of the figure is shown, for the interval $[0, \pi]$). As a function of θ, this function is clearly $\pi/4$-periodic, which reflects the eightfold symmetry. But one sees in fact several sets of four equidistant maxima, corresponding to characteristic scales a_j, and some of them are shifted by $\pi/8$. This is even clearer if one replaces the full measure μ_s by its skeleton [14, 21], which reduces here to the set of local modulus maxima (Fig. 8b). On this set of points, one can measure more precisely the successive characteristic scales a_j. Upon inspection, one may recognize *six* significant lines of maxima, corresponding, for $j = 1$ to $j = 6$ (bottom to top), to $\ln a_j = 0.32, 0.58, 0.95, 1.20, 1.81, 2.08$.

Consider first the three pairs of equidistant lines of maxima (1, 2), (3, 4), and (5, 6). In *each* pair, the ratio between the two successive scales is $\delta_1 = a_{j+1}/a_j \simeq 1.31 \simeq \sqrt{2} \cos(\pi/8)$, and the second line is shifted by $\pi/8$ from the first one. This means that one goes from the first line to the second by a rotation of $\pi/8$, combined with a dilation by a factor δ_1. In other words, the whole pattern has, in addition to its eightfold symmetry, a combined rotation–dilation symmetry. This is visible on the pattern itself: if one draws successive octagons, as shown in Fig. 9a, the dilation factor $\delta_1 = \sqrt{2} \cos(\pi/8)$ is easily obtained by a geometrical argument.

But there is more. Consider now the three lines of maxima $j = 2, 4, 5$, at $\ln a_j = 0.58, 1.20, 1.81$. These are obtained from one another by a rotation of $\pi/8$, combined with a dilation by a factor $\delta_2 = 1.85 \simeq 2 \cos(\pi/8)$. The same is true for lines 1 and 3. And, looking at the tiling, one readily observes that it is invariant under this second combined rotation–dilation symmetry also, as may be seen in Fig. 9b! The remarkable fact is that these two additional symmetries were discovered on the graph of the scale-angle measure, and *not* on the tiling itself!
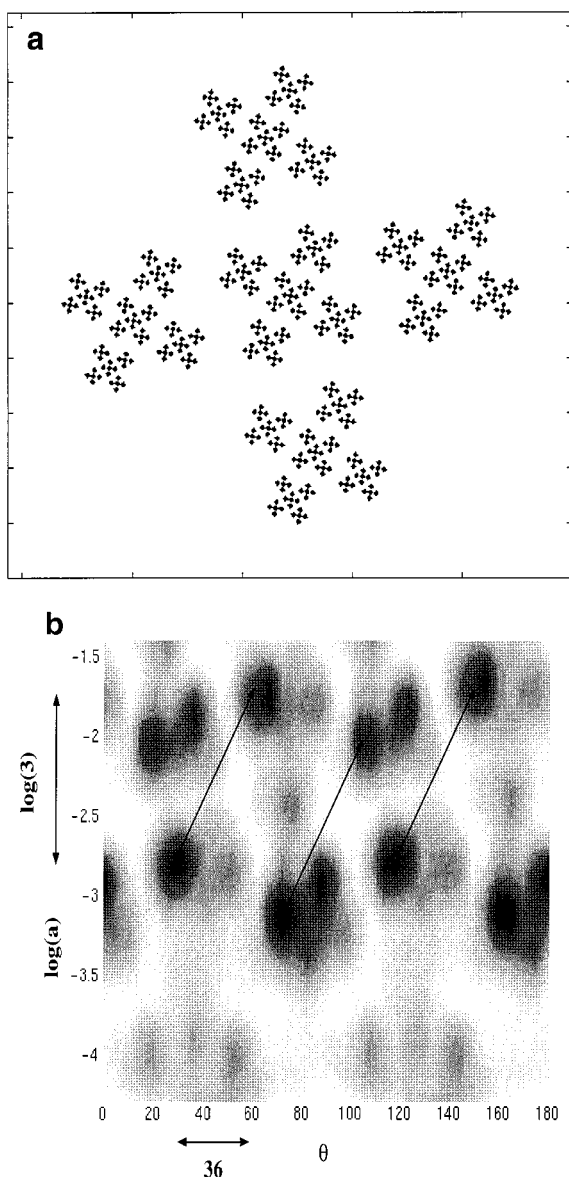
FIG. 6. Analysis of a pattern ("twisted snowflake") with a combined rotation–dilation symmetry: (a) the pattern; (b) the scale-angle measure $\mu_s(a, \theta)$, computed with a Cauchy wavelet $\psi_{44}^{(\mathscr{C}_{10})}$. Corresponding local maxima are shifted by 36° and a scaling ratio of 3.

At this stage, the method is still empirical. How are we sure that there is no *other* combined symmetry present in the tiling? This question may be answered by adapting a technique introduced by Hwang and Mallat [23] in the context of the wavelet analysis of multifractals. The idea is to determine the (exact or approximate) renormalization parameters of a given 1-D multifractal by a voting algorithm on the CWT, or its skeleton. In our case, this means writing the algorithm in the (a, θ) plane of the scale-angle measure. The procedure runs as follows.
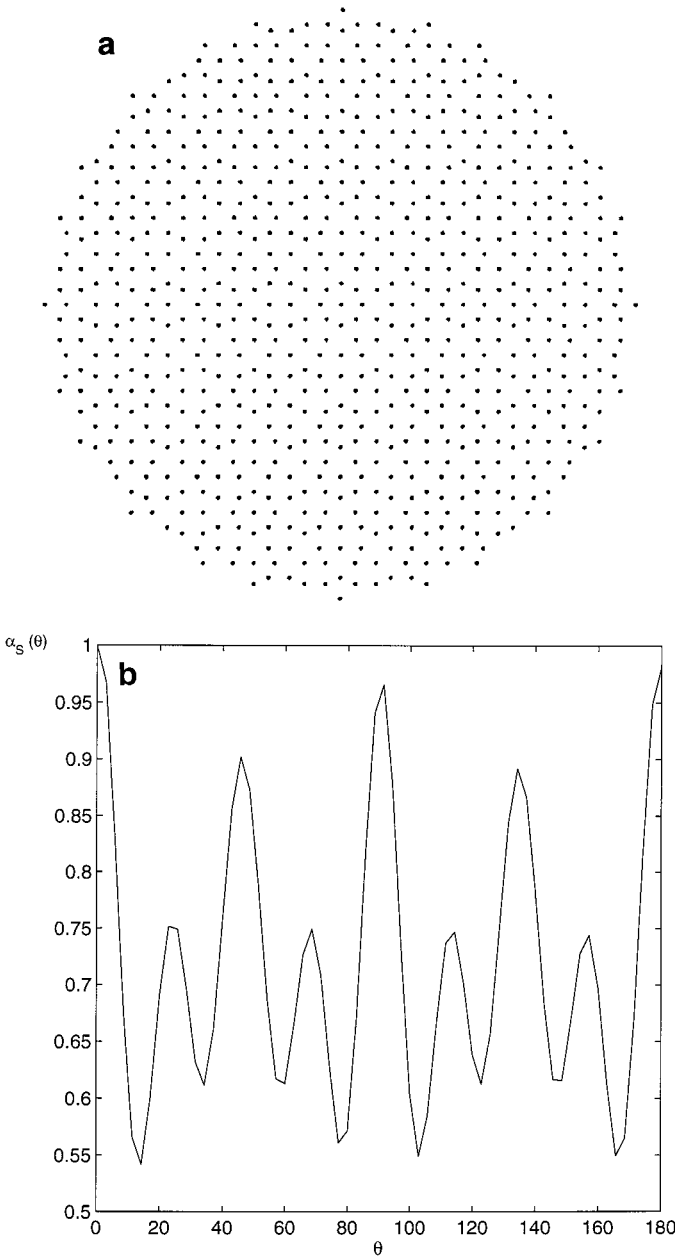
FIG. 7. Analysis of an octagonal tiling: (a) the tiling; (b) its angular measure $\alpha_s(\theta)$, showing the $\pi/4$ periodicity.

• First we pass to logarithmic coordinates for the scaling variable, $a = e^t$, and write the scale-angle measure of the signal s as $\mu_s(t, \theta)$. The renormalization operations on the signal are given by

$$L(\tau, \alpha)s(\vec{x}) = e^{-\tau}s(e^{-\tau}r_\alpha\vec{x}), \tag{5.3}$$
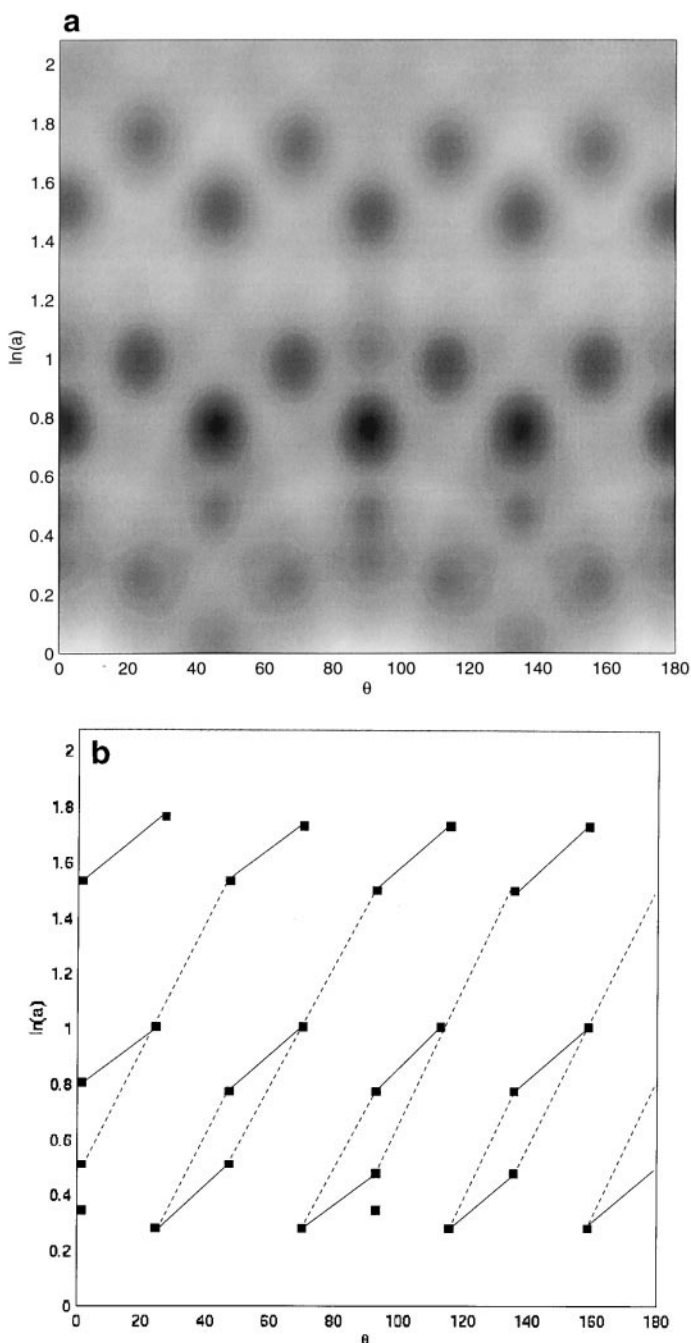
FIG. 8. Further analysis of the octagonal tiling: (a) its scale-angle measure $\mu_s(a, \theta)$; (b) the skeleton of the latter, which consists of six successive lines of four equidistant local maxima. Lines 2, 4, and 6 are obtained from lines 1, 3, and 5, respectively, by a rotation of $\pi/8$ combined with a dilation by δ_1. In the same way, lines 4 and 5 result from line 2 by repeated applications of the operation $\rho_2 = (\delta_2, \pi/8)$. Similarly for lines 1 and 3. For better visibility, homologous maxima are linked by a line segment, continuous for δ_1 and dashed for δ_2.
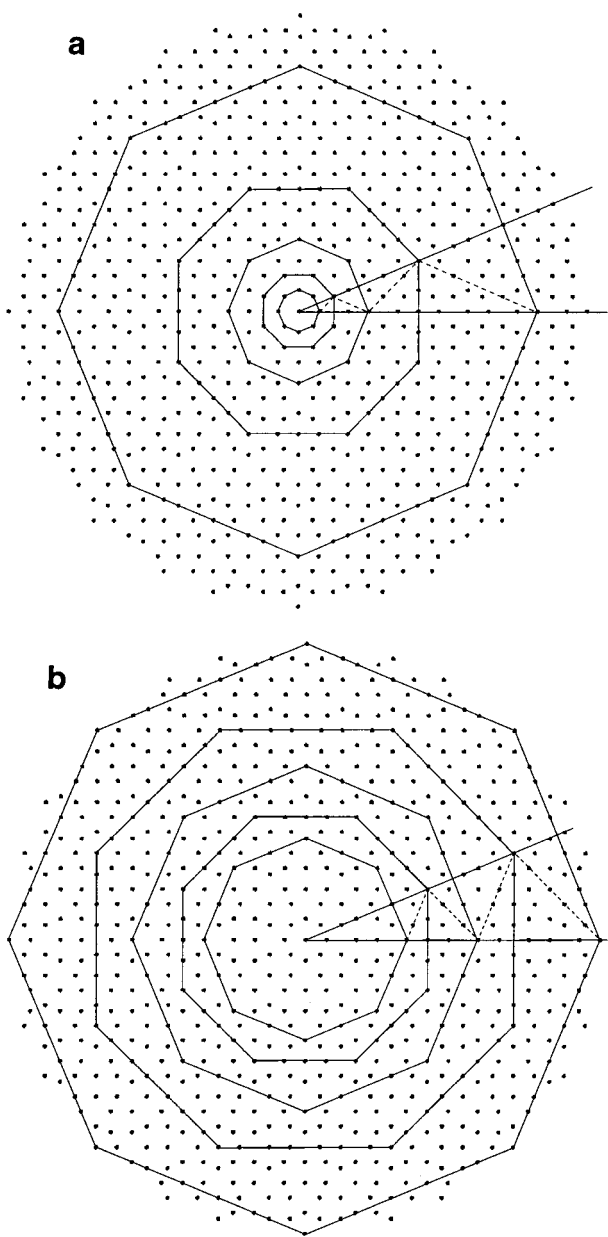
FIG. 9. Two sets of octagons on the octagonal tiling obtained by successive applications of a rotation by $\pi/8$ combined with a dilation by $\delta_1 = \sqrt{2}\,\cos(\pi/8)$ (a) and $\delta_2 = 2\cos(\pi/8)$ (b).

and from this we get

$$\mu_{L(\tau,\alpha)s}(t,\theta) = \mu_s(t - \tau, \theta - \alpha). \tag{5.4}$$

• Next the parameter space $[t_{\min}, t_{\max}] \times [\theta_{\min}, \theta_{\max}]$ is discretized on a linear grid Γ. For each pair $(\tau_0, \alpha_0) \in \Gamma$, we compute $\bar{\mu}_s(t,\theta) = \mu_s(t - \tau_0, \theta - \alpha_0)$ (this requires only shifting rows and columns of the matrix $\{\mu_s(i,j)\}$).

- Then evaluate

$$P(\tau_0, \alpha_0) = \|s\|_2^{-2} \int_{t_{min}}^{t_{max}} dt \int_{\theta_{min}}^{\theta_{max}} d\theta \tilde{\mu}_s(t, \theta) \mu_s(t, \theta). \tag{5.5}$$

Finally the algorithm says: Fix a constant $K > 0$. Then, if $P(\tau_0, \alpha_0) \geq K$, do $V(\tau_0, \alpha_0)$:= $V(\tau_0, \alpha_0) + 1$, where $V(\tau_0, \alpha_0)$ is the voting matrix, indexed by Γ and initialized as the null matrix.

- Once a vote has been cast for a point (τ_0, α_0), identify all its integer multiples $(n\tau_0, n\alpha_0)$ that lie within Γ, and give all their votes to (τ_0, α_0). In other words, one identifies the renormalization operations $L(\tau_0, \alpha_0)$ and $L^n(\tau_0, \alpha_0)$ for all $n \in \mathbb{N}_*$.
- Then proceed to the next renormalization point, if any, and repeat the previous operation.

The result is a voting matrix whose nonzero entries correspond exactly to all values of the renormalization parameters admitted by the signal. Note that errors may be included, by declaring that a vote is cast for (τ_0, α_0) if $P(\tau_0 \pm \tau_c, \alpha_0 \pm \alpha_c) \geq K$, where τ_c and α_c are fixed parameters. In this way small errors may be taken into account (this is usually called renormalization noise), for instance, those coming from sampling on a Cartesian grid in order to perform a FFT (this is the infamous gridding problem of NMR imaging).

This method has been applied to the skeleton given in Fig. 8b. The result is given in Fig. 10, which shows the renormalization parameters $\rho = (\delta, \theta)$ of the figure (for better visibility, we have added some of their multiples). This means that the latter is self-similar after a dilation by a factor δ combined with a rotation of θ. Of course the whole diagram is $\pi/4$-periodic, so that only five points are relevant: a pure rotation $(1, \pi/4)$; a pure dilation $\rho_0 = (\delta_0, 0)$, with $\delta_0 = 1 + \sqrt{2}$; and three combined operations $\rho_1 = (\delta_1, \pi/8)$, $\rho_2 = (\delta_2, \pi/8)$, and $\rho_3 = (\delta_3, \pi/8)$, where $\delta_3 = (2 + \sqrt{2})\cos(\pi/8)$. Taking into account the $\pi/4$-periodicity, we see that the product $\rho_1 \cdot \rho_2$ coincides with ρ_0, and furthermore, $\rho_3 = \rho_0 \cdot \rho_1$. In other words, there are no additional hidden symmetries.

As a matter of fact, the symmetry structure of the tiling is even more intricate. A closer inspection reveals that it is invariant under the combined operation δ_2-dilation + rotation and that this operation generates a semigroup (every point has a successor, but not necessarily a predecessor; i.e., the inverse operation is not a symmetry). This semigroup has apparently infinitely many different orbits (on the portion of the tiling visible in the figure, we have detected 10 different orbits). However, the other combined operation, δ_1-dilation + rotation, is *not* an exact symmetry; it is only approximate. For instance, some orbits stop after a few iterations, or have gaps (this feature is easily observed in Fig. 9b, by visualizing the orbit of the summit of a given octagon). Clearly a systematic study would be needed here. In fact, the tiling analyzed here is closely related to the 2-D quasicrystals, based on Pisot cyclotomic numbers, studied by Barache [7, 8]. Further results in this direction will be discussed elsewhere.

In addition to the intricate geometry of the tiling, one may notice some irregularities in the pattern of μ_s, which are attributable to the numerical treatment. Indeed, although the original tiling is perfectly regular, it is slightly distorted in order to fit a Cartesian grid, as required by the FFT algorithm used in the computation of the WT, and this creates some defects.
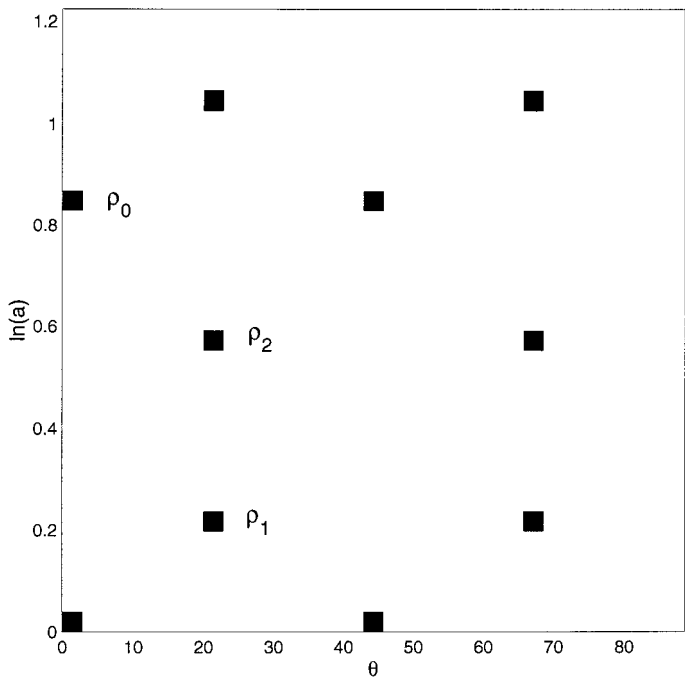
FIG. 10.   The set of renormalization parameters $\rho = (\delta, \theta)$ obtained by the voting algorithm on the skeleton of the WT of the octagonal tiling, given in Fig. 8b. The point on the horizontal axis corresponds to the $\pi/4$-periodicity. The points ρ_1 and ρ_2 correspond to the combined rotation–dilation operations with dilation ratio δ_1 and δ_2, respectively, whereas ρ_0 is a pure dilation, equivalent to the product $\rho_1 \cdot \rho_2$ under the $\pi/4$-periodicity. The other, unmarked, points are translates of the previous ones under both periodicities, in a and θ, and are added for better readability of the diagram.

Incidentally, these examples show why it is safer to integrate over all scales in order to isolate the angular behavior, rather than fix a certain scale $a = a_0$ and consider $\mu_s(a_0, \theta)$. If a_0 coincides with one of the characteristic scales, $a_1, a_2, \ldots$, the result is correct, but if a_0 falls in between, no maximum will be seen, and the symmetry is not detected. The effect is shown in Fig. 11 for the octagonal tiling of Fig. 7.

More important, the use of a *directional* wavelet is essential here. Suppose we perform the same analysis with an isotropic wavelet. Then the scale-angle measure no longer depends on θ; it reduces to a function $\beta_s(a)$ of a alone. Figure 12 shows the result for the tiling of Fig. 7. In Fig. 12a, we plot $\ln \beta_s(a)$ as a function of $\ln a$, together with the best linear fit, and in Fig. 12b, we plot the difference between the two, which represents the fluctuations around the linear trend. Now, if the pattern is invariant under dilation by a factor δ, it may be shown that these fluctuations are δ-periodic. This technique is often used for determining the inflation invariances of a 1-D quasiperiodic tiling, or the scaling factor of a fractal [6]. In the present case, three features are visible on the fluctuations shown in Fig. 12b. First, there is a repetition with period $\delta_0 = 1 + \sqrt{2}$, corresponding to the global dilation invariance. In addition, there are two less prominent repetitions, with ratios δ_1, δ_2. Clearly these scale ratios have a special role in the pattern, but such an analysis, ignoring the rotation angles, is unable to determine it without ambiguity. In other

$\mu_S(a_0, \theta)$

θ

$\mu_S(a_0, \theta)$

θ
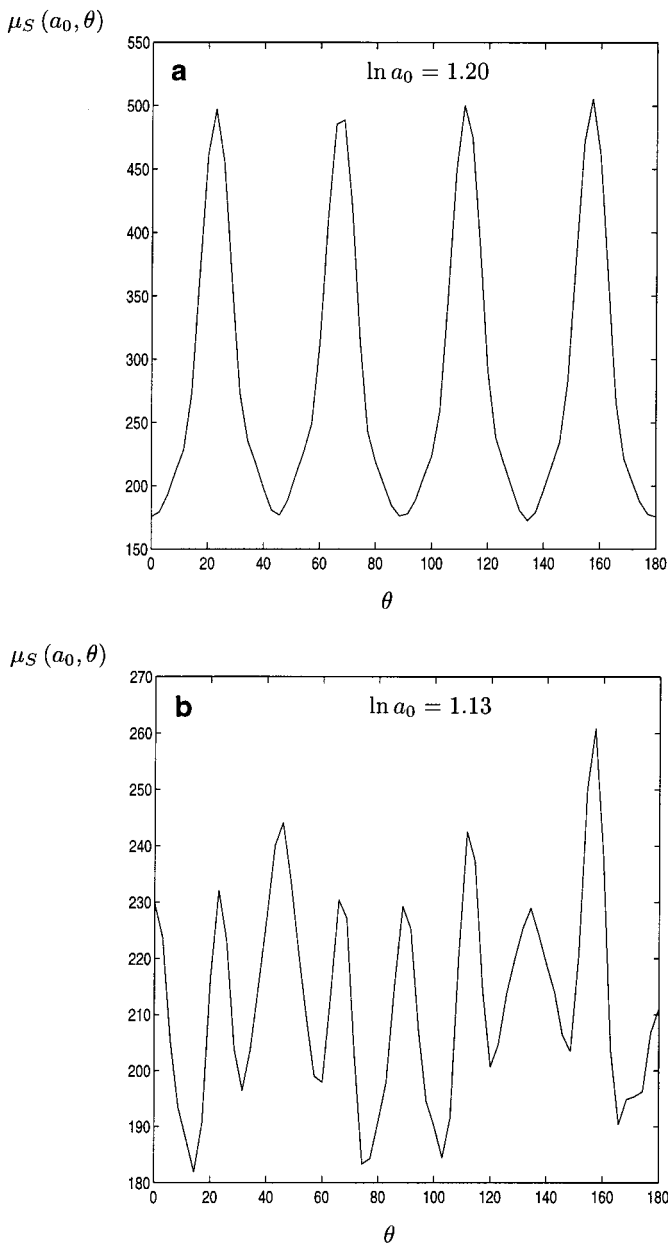
FIG. 11. The scale-angle measure of the octagonal tiling from Fig. 7, for fixed values a_0 of the scale: (a) for $\ln a_0 = 1.20$, on a line of maxima, the periodicity is obvious; (b) for $\ln a_0 = 1.13$, between two lines of maxima, the symmetry is not seen.

words, detecting combined dilation–rotation invariances of the pattern requires a directional wavelet, which allows one to exploit the full power of the scale-angle measure.

In conclusion, we have obtained a method for determining, in a straightforward and economical way, the (possibly hidden) symmetries of a given pattern. Of course, rotational symmetry is easy and there are various methods for determining it. But, as far as we know,
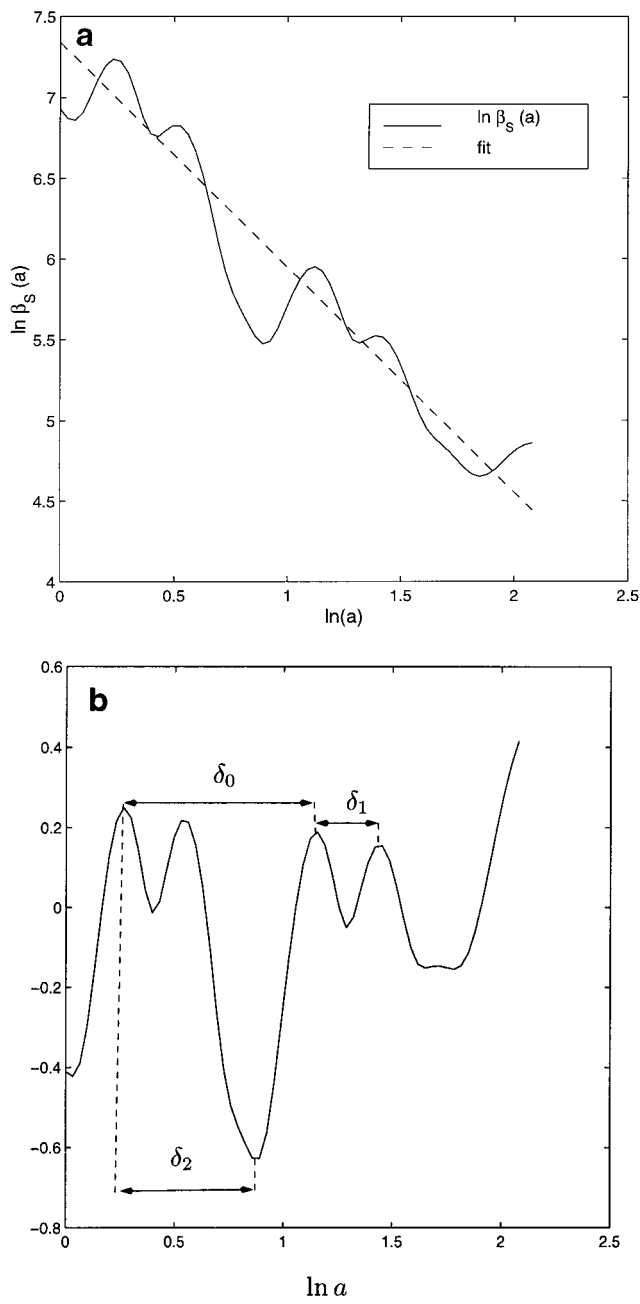
FIG. 12. Fluctuations of the scale measure β_s: (a) $\ln \beta_s(a)$ as a function of $\ln a$, together with the best linear fit; (b) fluctuations of $\beta_s(a)$ around the linear fit—the three scaling factors δ_0, δ_1, and δ_2 are visible.

no method exists for determining the combined dilation–rotation invariances of a given pattern. Moreover, this applies not only to a genuine lattice, but also to a quasilattice, for which the symmetry is only local. The reason is that the local character of the wavelet transform allows one precisely to treat exact and local symmetries on the same footing.

A typical application is the diffraction pattern of a quasicrystal [20, 26], which exhibits a local n-fold point symmetry, with $n = 5, 8, 10$, or 12 (all forbidden as an exact symmetry by the laws of crystallography, because they are incompatible with translational invariance). In addition, these diffraction patterns are organized into constellations of bright Bragg spots of unequal intensity, which are self-similar with an irrational scaling factor, namely:

- $\delta = 2 \cos(2\pi/10) = \frac{1}{2}(1 + \sqrt{5}) \equiv \tau$ (the golden mean), for $n = 5, 10$;
- $\delta = 1 + 2 \cos(2\pi/8) = 1 + \sqrt{2}$, for $n = 8$;
- $\delta = 2 + 2 \cos(2\pi/12) = 2 + \sqrt{3}$, for $n = 12$.

Similar structures are observed on quasicrystal surfaces by scanning microscopy. Thus our octagonal tiling has the same global symmetries as the $n = 8$ quasicrystals, but in addition it has the two combined dilation–rotation invariances discussed above. It would be interesting to find similar helicoidal symmetries in genuine quasicrystals and understand their physical origin.

More generally, the scale-angle measure is a natural tool for studying self-similar tilings [7, 8]. These patterns have invariance properties under (discrete) rotations and dilations, but *no* translation invariance. In fact they can be characterized solely by their dilation–rotation renormalization parameters, as discussed above in a particular example. Thus the space dependence of the wavelet transform is irrelevant for analyzing them, and it may be averaged upon, as we precisely did in (5.1). Further work in this direction is in progress.

Needless to say, directional wavelets, and in particular Cauchy wavelets, may be applied in other instances where high directional selectivity is needed. For instance, one of us (R.M.) is currently applying them to the detection and classification of targets in forward looking infrared imagery (FLIR). The preliminary results look very promising.

ACKNOWLEDGMENTS

REFERENCES

1. J.-P. Antoine, P. Carrette, R. Murenzi, and B. Piette, Image analysis with two-dimensional continuous wavelet transform, *Signal Process.* **31** (1993), 241–272.

2. J.-P. Antoine and R. Murenzi, Two-dimensional directional wavelets and the scale-angle representation, *Signal Process.* **52** (1996), 259–281.

3. J.-P. Antoine, R. Murenzi, and P. Vandergheynst, Two-dimensional directional wavelets in image processing, *Internat. J. Imaging Syst. Technol.* **7** (1996), 152–165.

4. J.-P. Antoine and R. Murenzi, Two-dimensional continuous wavelet transform as linear phase space representation of two-dimensional signals, *in* "Wavelet Applications IV" (SPIE 1997 Symposium on Aerospace/Defense Sensing, Simulation, and Controls, Orlando, Apr. 1997), **3078** (1997), 206–217.

5. F. Argoul, A. Arnéodo, J. Elezgaray, G. Grasseau, and R. Murenzi, Wavelet analysis of the self-similarity of diffusion-limited aggregates and electrodeposition clusters, *Phys. Rev. A* **41** (1990), 5537–5560.

6. A. Arnéodo, F. Argoul, E. Bacry, J. Elezgaray, E. Freysz, G. Grasseau, J. F. Muzy, and B. Pouligny, Wavelet transform of fractals, *in* "Wavelets and Applications" (Y. Meyer, Ed.), pp. 286–352, Springer-Verlag, Berlin; Masson, Paris, 1991.

7. D. Barache, "Propriétés algébriques et spectrales des structures apéiodiques," Thèse de Doctorat, Université Paris 7, 1995.

8. D. Barache, B. Champagne, and J.-P. Gazeau, Pisot-cyclotomic quasilattices and their symmetry semi-groups, *in* "Quasicrystals and Discrete Geometry" (J. Patera, Ed.), pp. 15–66, Fields Institute Monographs, Amer. Math. Soc., Providence, RI, 1998.

9. C. Cohen-Tannoudji, B. Diu, and F. Laloë, "Mécanique Quantique, Tome I." Hermann, Paris, 1977.

10. S. Dahlke and P. Maass, The affine uncertainty principle in one and two dimensions, *Comput. Math. Appl.* **30** (1995), 293–305.

11. T. Dallard and G. R. Spedding, 2-D wavelet transforms: Generalization of the Hardy space and application to experimental studies, *European J. Mech. B Fluids* **12** (1993), 107–134.

12. I. Daubechies, "Ten Lectures on Wavelets," SIAM, Philadelphia, 1992.

13. I. Daubechies and Th. Paul, Time-frequency localisation operators—A geometric phase space approach. II. The use of dilations, *Inverse Problems* **4** (1988) 661–680.

14. N. Delprat, B. Escudié, P. Guillemain, R. Kronland-Martinet, Ph. Tchamitchian, and B. Torrésani, Asymptotic wavelet and Gabor analysis: Extraction of instantaneous frequencies, *IEEE Trans. Inform. Theory* **38** (1992), 644–664.

15. W. T. Freeman and E. H. Adelson, The design and use of steerable filters, *IEEE Trans. Pattern Anal. Machine Intell.* **13** (1991), 891–906.

16. D. Gabor, Theory of communication, *J. Inst. Electr. Engrg. (London)* **93** (1946) 429–457.

17. K. Gottfried, "Quantum Mechanics. Vol. I: Fundamentals," Benjamin, New York/Amsterdam, 1966.

18. C. Gonnet and B. Torrésani, Local frequency analysis with two-dimensional wavelet transform, *Signal Process.* **37** (1994), 389–404.

19. A. Grossmann and J. Morlet, Decomposition of Hardy functions into square integrable wavelets of constant shape, *SIAM J. Math. Anal.* **15** (1984), 723–736.

20. P. Guyot, P. Kramer, and M. de Boissieu, Quasicrystals, *Rep. Prog. Phys.* **54** (1991), 1373–1425.

21. Ph. Guillemain, R. Kronland-Martinet, and B. Martens, Estimation of spectral lines with the help of the wavelet transform. Applications in N.M.R. spectroscopy, *in* "Wavelets and Applications" (Y. Meyer, Ed.), pp. 38–60, Springer-Verlag, Berlin; Masson, Paris, 1991.

22. M. Holschneider, "Wavelets, An Analysis Tool," Oxford Univ. Press, Oxford, 1995.

23. W.-L. Hwang and S. Mallat, Characterization of self-similar multifractals with wavelet maxima, *Appl. Comput. Harmon. Anal.* **1** (1994), 316–328.

24. W.-L. Hwang, C.-S. Lu, and P.-C. Chung, Shape from texture: Estimation of planar surface orientation through the ridge surfaces of continuous wavelet transform, *IEEE Trans. Image Process.* **7** (1998), 773–780.

25. A. K. Jain and F. Farrokhnia, Unsupervised texture discrimination using Gabor filters, *J. Pattern Recogn.* **24** (1991), 1167–1186.

26. C. Janot, "Quasicrystals, A Primer," Oxford Univ. Press, Oxford, 1994.

27. J. R. Klauder, Path integrals for affine variables, *in* "Functional Integration, Theory and Applications" (J.-P. Antoine and E. Tirapegui, Eds.), pp. 101–119, Plenum Press, New York/London, 1980.

28. J. R. Klauder and B. S. Skagerstam, "Coherent States—Applications in Physics and Mathematical Physics," World Scientific, Singapore, 1985.

29. C.-S. Lu, W.-L. Hwang, H.-Y. M. Liao, and P.-C. Chung, Shape from texture based on the ridge of continuous wavelet transform, *in* "Proc. IEEE Intern. Conf. on Image Processing (ICIP-96), Lausanne, Sept. 1996" (P. Delogne, Ed.), Vol. I, pp. 291–294, IEEE, Piscataway, NJ, 1996.

30. Th. Paul, "Ondelettes et Mécanique Quantique," Thèse de doctorat, Université d'Aix-Marseille II, 1985.

31. Th. Paul and K. Seip, Wavelets in quantum mechanics, *in* "Wavelets and Their Applications" (M. B. Ruskai, G. Beylkin, R. Coifman, I. Daubechies, S. Mallat, Y. Meyer, and L. Raphael, Eds.), pp. 303–322, Jones and Bartlett, Boston, 1992.

32. S. C. Pei and S.-B. Jaw, Two-dimensional general fan-type FIR digital filter design, *Signal Process.* **37** (1994), 265–274.

33. P. Perona, Steerable–scalable kernels for edge detection and junction analysis, *Image Vision Comput.* **10** (1992), 663–672.

34. E. P. Simoncelli and H. Farid, Steerable wedge filters for local orientation analysis, *IEEE Trans. Image Process.* **5** (1996), 1377–1382.

35. E. P. Simoncelli, W. T. Freeman, E. H. Adelson, and D. J. Heeger, Shiftable multiscale transforms, *IEEE Trans. Inform. Theory* **38** (1992), 587–607.

36. E. M. Stein and G. Weiss, "Introduction to Fourier Analysis on Euclidean Spaces," Princeton Univ. Press, Princeton, NJ, 1971.

37. R. F. Streater and A. S. Wightman, "PCT, Spin and Statistics, and All That," Benjamin, New York, 1964.

38. D. Vu Giang and F. Móricz, Hardy spaces on the plane and double Fourier transforms, *J. Fourier Anal. Appl.* **2** (1996), 487–505.

39. A. B. Watson, The Cortex Transform: Rapid computation of simulated neural images, *Comput. Vision Graph. Image Process.* **39** (1987), 311–327; Efficiency of a model human image code, *J. Opt. Soc. Amer. A* **4** (1987), 2401–2417.

40. W. Wisnoe, "Utilisation de la méthode de transformée en ondelettes 2-D pour l'analyse de visualisation d'écoulements," Thèse de Doctorat ENSAE, Toulouse, 1993.

41. W. Wisnoe, P. Gajan, A. Strzelecki, C. Lempereur, and J.-M. Mathé, The use of the two-dimensional wavelet transform in flow visualization processing, *in* "Progress in Wavelet Analysis and Applications" (Y. Meyer and S. Roques, Eds.), pp. 455–458, Ed. Frontières, Gif-sur-Yvette, 1993.

42. A. P. Witkin, Scale-space filtering, *in* "Proc. 8th Int. Joint Conf. on Artif. Intell.," Karlsruhe, Aug. 1983.